Comparison between above-water and in-water determinations of the water-leaving radiance (Case 1 waters) in the frame of the **BOUSSOLE** project.

David ANTOINE, Alec SCOTT, Bernard GENTILI

Laboratoire d'Océanographie de Villefranche (LOV), 06238 Villefranche sur mer cedex, FRANCE

BOUSSOLE project
ESA/ESTEC contract N° 14393/00/NL/DC
CCN (rider) #2

June 23, 2004

Foreword

This report is the result of a collaborative effort between the LOV ("*Laboratoire d'Océanographie de Villefranche*"), the LOA ("*Laboratoire d'Optique Atmosphérique*" in Lille) and the LISE ("*Laboratoire Interdisciplinaire en Sciences de l'Environnement''*, in Wimereux). The work presented here is based on the use of data collected at the BOUSSOLE site. This report is part of the technical report series that is being established by the BOUSSOLE project. The comments and conclusions provided in this report are those of the authors. In no way they express the position of the Agencies or institutions cited below.

BOUSSOLE is funded/supported by the following Agencies, Institutions or Programs :

European Space Agency

Centre National d'Etudes Spatiales, France

National Aeronautics and Space Administration of the USA

The NASA' SIMBIOS project

Centre National de la Recherche Scientifique, France

Institut National des Sciences de l'Univers, France

Université Pierre & Marie Curie, France

Observatoire Océanologique de Villefranche sur mer, France

Table of contents

1   Introduction

1.1   *Context, general goal*

The validation of the "geophysical products" derived from observations of the satellite ocean colour sensors requires the collection of the same parameters from *in situ* instrumentation. In this report, we focus on the validation of the water-leaving reflectance, and we examine a protocol issue, which is linked to the different ways of deriving at sea a water-leaving reflectance value that is suitable for the validation of this product as it is derived in particular from the MERIS ocean colour sensor observations (see at http://www.envisat/esa.int).

The two techniques that we have tested use two very different instrument types. The first one measures the upwelling irradiance in the water column in a free-fall profiling mode, using a multi-channel submersible radiometer (see section 3 for the detailed instrument description). During the profiling, the above-water downwelling irradiance is recorded on deck. Extrapolation of the vertical profile of irradiance allows the irradiance value just below the water-air interface to be determined. The above-water reference is corrected for the transmission from air to just below the sea surface, which allow the ratio of upwelling to downwelling irradiances to be formed at null depth. This is the reflectance, noted R. Deriving the water-leaving reflectance in a given viewing direction then requires the knowledge of the Q factor (Morel and Gentili, 1993), *i.e.*, the upwelling irradiance to upwelling radiance ratio.

The second technique measures directly the water-leaving radiance exiting the ocean at a nadir angle of about 40° and an azimuth difference with respect to the sun position of about 135°, as well as the sky radiance reflected in the same viewing direction by the wind-roughened sea surface, plus a small, albeit unavoidable, contribution from combined reflection on the ship superstructure and the sea surface. The instrument is a portable hand-held radiometer that has been designed for that purpose (Fougnie et al., ???; again see section 3 for the detailed instrument description). It is called the SIMBADA, and is an evolution of the former SIMBAD radiometer (see at http://www-loa.univ-lille1.fr/recherche/ocean_color/src).

Inter-comparison between above-water and in-water techniques have been already performed several times elsewhere using other instrument types (Frouin *et al*., 2000; Toole *et al*., 2000; Hooker *et al*., 2002; Zibordi *et al*., 2002), and sometimes with a considerable amount of details and with extremely controlled procedures (Hooker and Morel, 2002). The aim of the latter work was precisely to examine the effects of various perturbations that interplay in forming the signal measured from above the sea surface, and to assess their importance in the final error budget of such measurements, as well as the ability we have (or we don't have) to correct for these perturbing effects.

It was not our goal here to repeat such studies, and rather the work reported here had two very specific goals, as follows :

(1) The SIMBADA radiometer is a newly developed instrument, and the processing of its measurements as well uses quite new concepts. Both the instrument and the data processing code need some qualification with respect to other instruments whose history is longer and which are better understood thanks to intensive use in marine optics work in the past decades. We aim at providing some elements to help in this qualification process. This includes possible improvements in the data processing procedures.

(2) The suitability of using the SIMBADA from the Téthys-II research vessel (see next sections) remains to be established, when the collected data are to be used for the validation of the water-leaving reflectance products derived from the MERIS observations. Indeed, the ship perturbations, which have been identified as being sometimes preventing the derivation of the water-leaving reflectance with the desired accuracy (Hooker and Morel, 2003), are by definition specific to the ship. A specific work was therefore needed in the context of the BOUSSOLE project.

1.2   *A short reminder about the accuracy we aim at when validating water-leaving reflectance*

The goal of the atmospheric correction applied to satellite ocean colour observations is to retrieve the water-leaving reflectance at the sea level from the total reflectance recorded at the top of the atmosphere (TOA). The water-leaving reflectances transmitted through the atmosphere form at the TOA level what is called the "marine reflectances". These reflectances are thus made of photons that have crossed the atmosphere down to the ocean, then have twice crossed the air-sea interface before reaching the sensor

after a second atmospheric travel. The spectrum of the water-leaving reflectances carries information about the bio-optical state of the oceanic upper layers.

Because the atmospheric contribution largely exceeds the contribution of the ocean (in a ratio of about 10/1), the former needs to be accurately assessed for the final objective to be reachable. This accuracy has been previously determined (e.g., Gordon, 1997; Antoine and Morel, 1999), and can be expressed in slightly different terms, leading to a set of requirements that should be fulfilled. Note that these requirements are expressed in terms of uncertainties, rather than in terms of accuracy. These requirements concern on the one hand the retrieval of the water-leaving reflectance at a given wavelength, whatever the use of this data in subsequent analyses, and, on the other hand, the retrieval of the chlorophyll concentration from some parts of the water-leaving reflectance spectrum.

A first requirement is a 5% uncertainty in the blue domain (*i.e.*, around 443 nm) and for oligotrophic waters (*i.e.*, chlorophyll concentration < 0.1 mg m^{-3}), which is supposed to maintain the capability of accurately computing the chlorophyll concentration in such a situation where the signal in the blue is maximum (Gordon, 1997).

Another way of expressing these requirements is in terms of reflectance error. We use here the values determined in Antoine and Morel (1999). In terms of the retrieval of 30 reflectance values, the requirement is that atmospheric correction errors be maintained within ± 1-$2\ 10^{-3}$ at 443 nm, within $\pm 5\ 10^{-4}$ at 490 nm, and within $\pm 2\ 10^{-4}$ at 560 nm. Note that this last value at 560 nm is equal to the "noise equivalent reflectances" specified for MERIS. If it is assumed that atmospheric correction errors in the 440-500 nm domain are about twice the errors at 560 nm, the requirement associated to the discrimination of 30 (Chl) values is that errors remain within $\pm 1\ 10^{-3}$ at 443 nm (then $\pm 5\ 10^{-4}$ at 560 nm), or within $\pm 5\ 10^{-4}$ at 490 nm (then $\pm 2\ 10^{-4}$ at 560 nm). When expressed as relative errors, all the above requirements represent about 1% of the normalised oceanic reflectances at 443 nm (and often 2-5%), except when (Chl) > 3 mg m^{-3}. The situation is about the same for the wavelength couple 490-560 nm.

2   Location : the BOUSSOLE site

The site where the inter-comparisons presented in this report were performed is situated by 43°22'N and 7°54'E, which is located in the Ligurian sea (Western Mediterranean sea, see map below; depth is 2440 meters). This site has been originally selected because currents are extremely low; this is because the site is nearly at the center of the cyclonic circulation of the Ligurian sea.

Oligotrophic conditions (Chl < 0.1 mg m^{-3}) prevail at this site in summer and occasionally in winter, while a reasonable range of Chl is attainable thanks to (1) a spring bloom with concentrations up to 2 mg m^{-3}, (2) a secondary and less intense bloom in fall, and (3) local enhancements in winter when sunny weather temporarily stabilises the nutrient-rich waters. The conditions prevailing during our optic casts are provided in section 6.
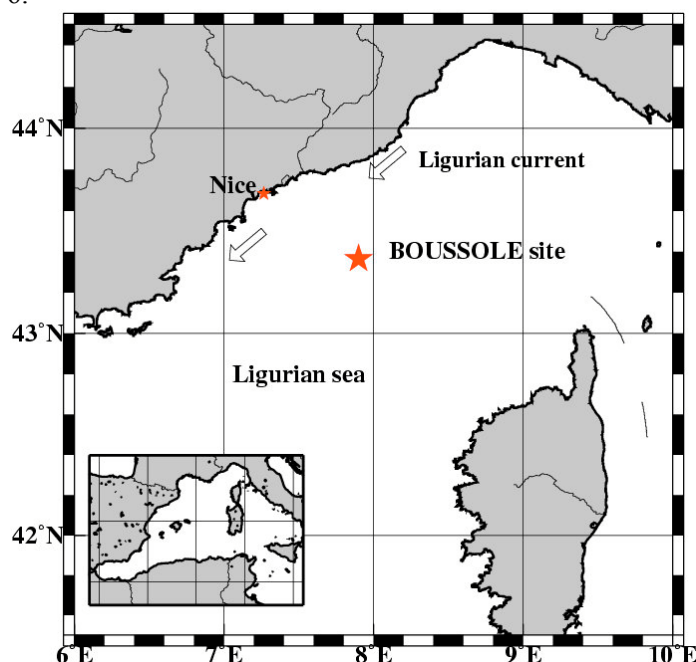

Fig. 1. Map of the BOUSSOLE site

3   Radiometers and their calibration

3.1   In-water radiometer : the Satlantic's SPMR & SMSR

The Satlantic' SPMR ("SeaWiFS Profiling Multichannel Radiometer") free-fall radiometer is used at LOV since 1995, and in tens of labs around the World for now 8 years. The "LOV version" of this profiling instrument is equipped with 2 "irradiance heads", collecting the upwelling and downwelling plane irradiances at the following λ : 412, 443, 456, 490, 510, 532, 560, 620, 665, 683, 705, 779, 865 nm.

The SPMR Profiler is made of a long pressure case (1.2 meters, 9 cm diameter) that contains the majority of system electronics, while the optical sensors are located and separately housed at either end of the case – looking up and down. The top end of the instrument has buoyant fins to stabilise the instrument's under-water free fall deployment and the bottom end has a small annular lead ballast to further stabilise the orientation and provide for fine tuning of the free fall velocity.

Heads used for measuring irradiance, in *mW/(cm 2 ·nm)*, have a black Delrin plate on the end. The plate contains 13 specially-designed, diffuser-based, cosine collectors (see Fig. 2). Tilt and pressure are recorded at the same frequency than the irradiance measurements, *i.e.*, at 6 Hz. The SPMR is accompanied by a deck reference sensor, called the "SMSR" ("SeaWiFS Multichannel Surface Reference"). This sensor is equipped with the same 13 wavelengths, and is based on the same electronics than the SPMR. Data acquisition is simultaneous between the SPMR and the SMSR and it is performed again at the same 6 Hz frequency.

The absolute calibration of the SPMR and SMSR with respect to NIST-traceable standards is performed every 6 months in the Satlantic optics calibration laboratory, and it is tracked between these absolute calibrations using at the LOV the ultra-stable portable light source developed for that purpose by Stalantic, *i.e.*, the "SeaWiFS Quality Monitor", SQM-II (Hooker and Aiken, 1998). Combining these two elements allows a 3% maximum uncertainty to be maintained on the calibration of the SPMR and SMSR.

Fig. 2. SPMR & SMSR pictures

The SPMR on the ship deck
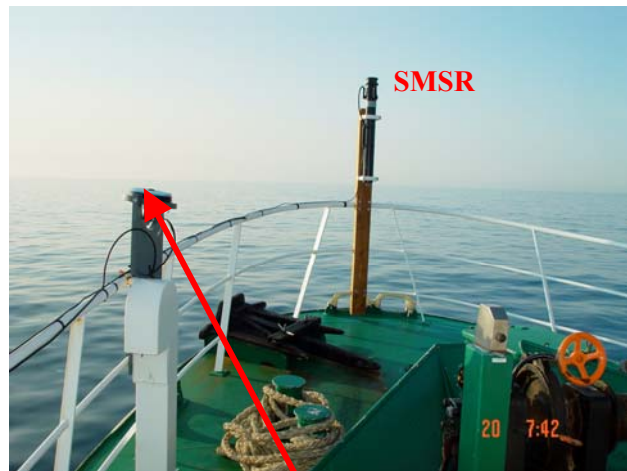
The deck reference ("SMSR") at the bow of the ship, plus a spherical PAR sensor used as a check of irradiance stability (put on a gimbal).

The SMSR head, with the 13 cosine collectors

SPMR/SMSR deck unit and the acquisition laptop.

3.2   *Above-water radiometer : the LOA' SIMBADA portable radiometer*

The SIMBADA instrument is an above-water radiometer designed and manufactured by the University of Lille, France. It is an upgraded version of the SIMBAD (reference ?) above water radiometer. It measures both water-leaving radiance and aerosol optical thickness in 11 spectral bands centred at 350, 380, 412, 443, 490, 510, 560, 620, 670, 750, and 870 nm by viewing the ocean surface (ocean-viewing mode) and the sun (sun-viewing mode) sequentially. The same optics (field-of-view of 3 degrees), interference filters, and detectors are used in both ocean-viewing and sun-viewing mode. Different electronic gains are used for each mode. The optics are fitted with a vertical polarizer, to reduce reflected skylight when the instrument is operated in ocean-viewing mode. A small GPS is now fixed in the front panel of the SIMBADA for automatic acquisition of geographic location at the time of measurement. Viewing angles are acquired automatically.

Viewing of the ocean must be made in clear sky conditions (3/4 of sky cloudless, and no clouds obscuring the sun), outside the sun glint region (relative angle between solar and viewing directions of 45 to 90 degrees), and at a nadir angle of about 45 degrees. For those angles, reflected skylight is minimised as well as residual ocean polarisation effects. The measurements can be made on a steaming ship so there is no need to stop the ship to make measurements. To normalise water-leaving radiance, incident solar irradiance is not measured, but computed using the aerosol optical thickness. The operator can select, in addition to ocean-viewing and sun-viewing modes, dark current and calibration modes. Each series of measurements lasts 10 seconds. Frequency of measurements is about 8 Hertz. Data is stored internally and downloaded onto diskette at the end of the day or a cruise. The instrument is powered by batteries that can be charged using a main supply of 110-240 V, 50hz-60hz. About 2 hours of charging should be enough for one day of measurements.

Fig. 3. SIMBADA pictures (see at http://www-loa.univ-lille1.fr/recherche/ocean_color/src/).

4   Deployment techniques

A SPMR profile starts when the instrument has reached a distance of 50 meters off the ship stern (the ship is 25 meters long and a mark on the cable indicates the 50 meters distance). The instrument is then released and falls at approximately 0.5 m s^{-1} in the water column, collecting data at a 6Hz frequency. The descent is stopped when the pressure sensor indicates a depth of about 150 meters, except in extremely clear waters where the profile is performed down to 200 meters. This technique allows to steer clear of the ship shadow, and to get measurements with tilt angles less than 2 degrees. The sun is usually on port side of the ship, which is anyway not so important precisely because the ship shadow is not affecting the measurements (see Fig. 4)
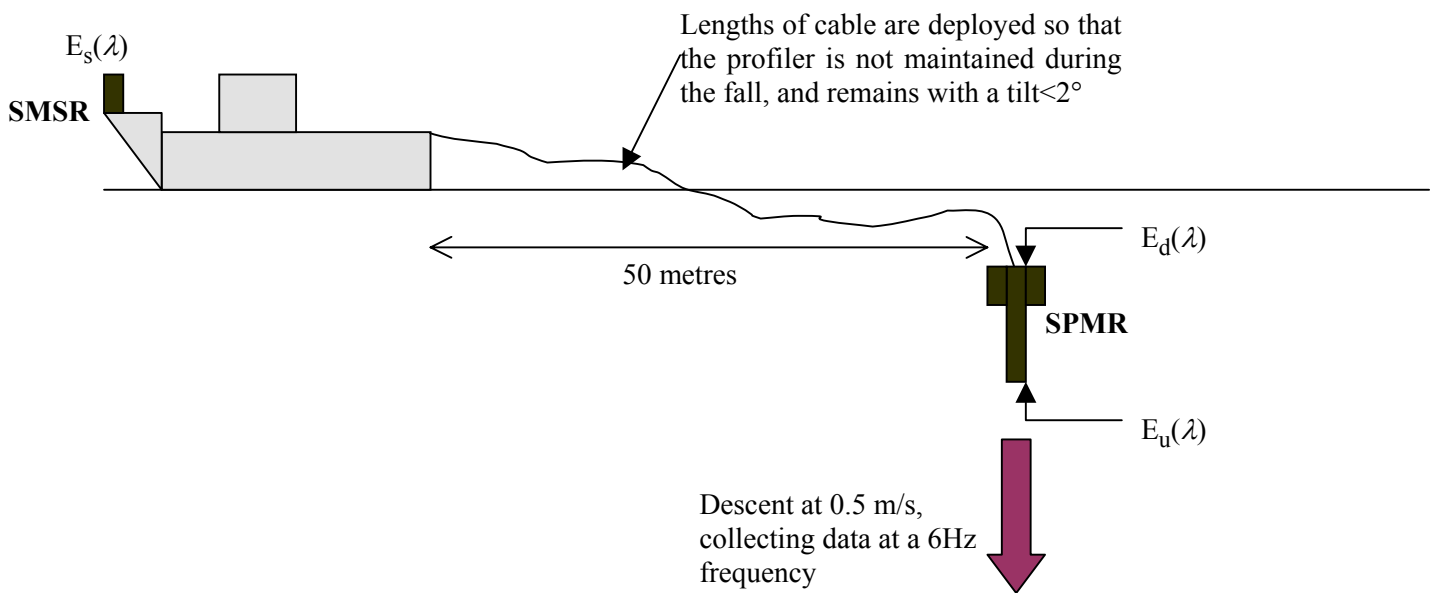
Fig. 4. Scheme of the SPMR deployment organisation

The SIMBADA has been used from the bow of the ship or from its upper superstructure when the weather was allowing to do so, which were the two more convenient locations where we were able to be sufficiently high above the sea surface. This is important, because any ship shadow effect or perturbation from reflection on the ship superstructure is minimised when increasing the vertical distance between the operator and the sea surface, and then the horizontal distance between the point of the sea surface which is aim at and the ship hull.

The full sequence of measurements was :

3 dark current recordings, each 10 seconds.
3 sun aiming, each of 10 seconds (for derivation of the aerosol optical thickness)
3 or 4 sea aiming, each of 10 seconds.
3 sun aiming, each of 10 seconds (for derivation of the aerosol optical thickness)
3 dark current recordings, each 10 seconds.

$L_w + \rho.L_{sky}$

Ship shadow

Ship stern

120 to 135 degrees

Direction of sun rays

Sun

45°

4 meters

~5 meters

Sun

Ship superstructure

Ship stern

SIMBADA radiometer

120 to 135 degrees

Ship shadow

Direction of sun rays

$L_w + \rho.L_{sky}$
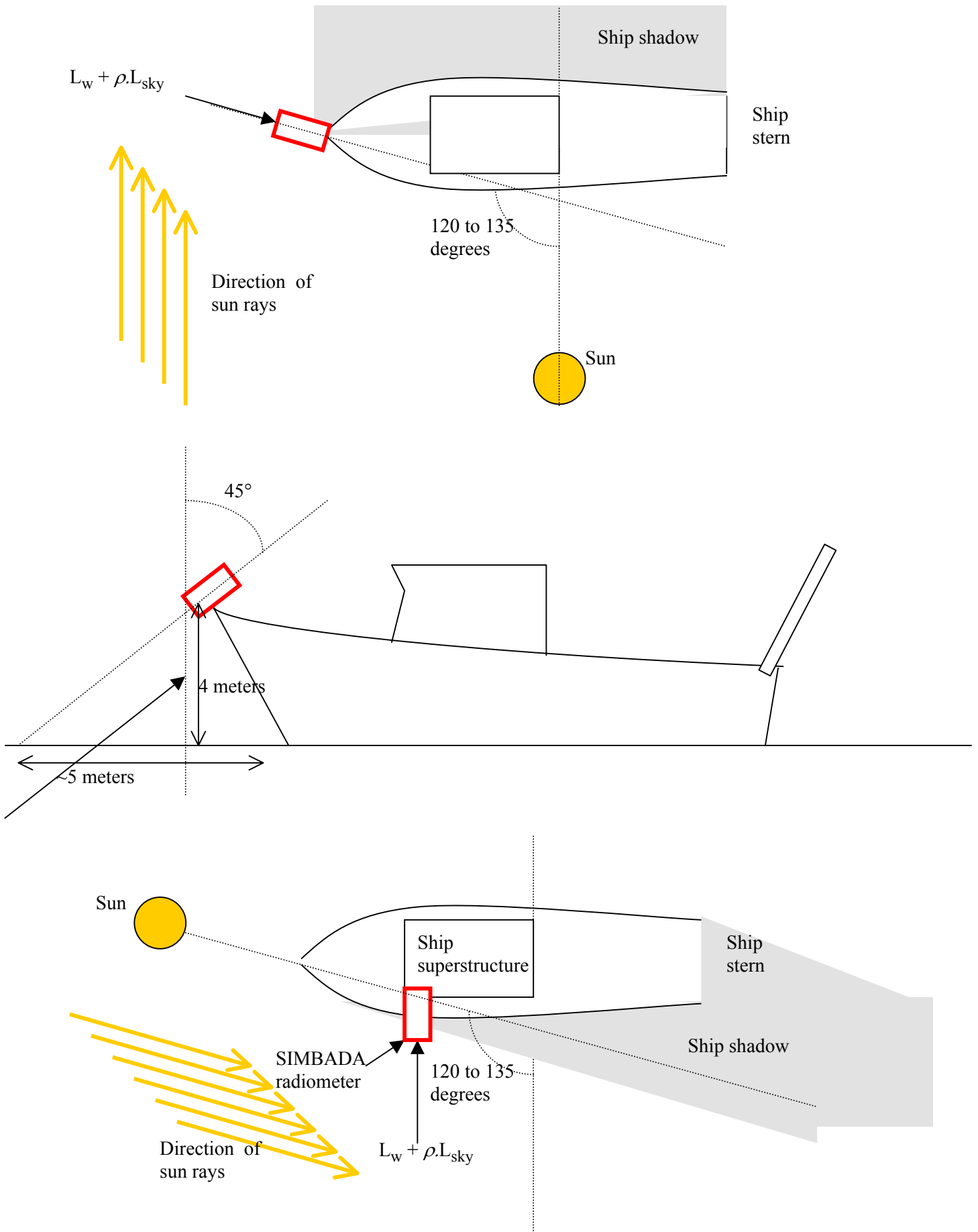
Fig. 5. Schemes of the SIMBADA deployment organisations (the SIMBADA is the red rectangular box)

Ship
superstructure

6 meters

45°
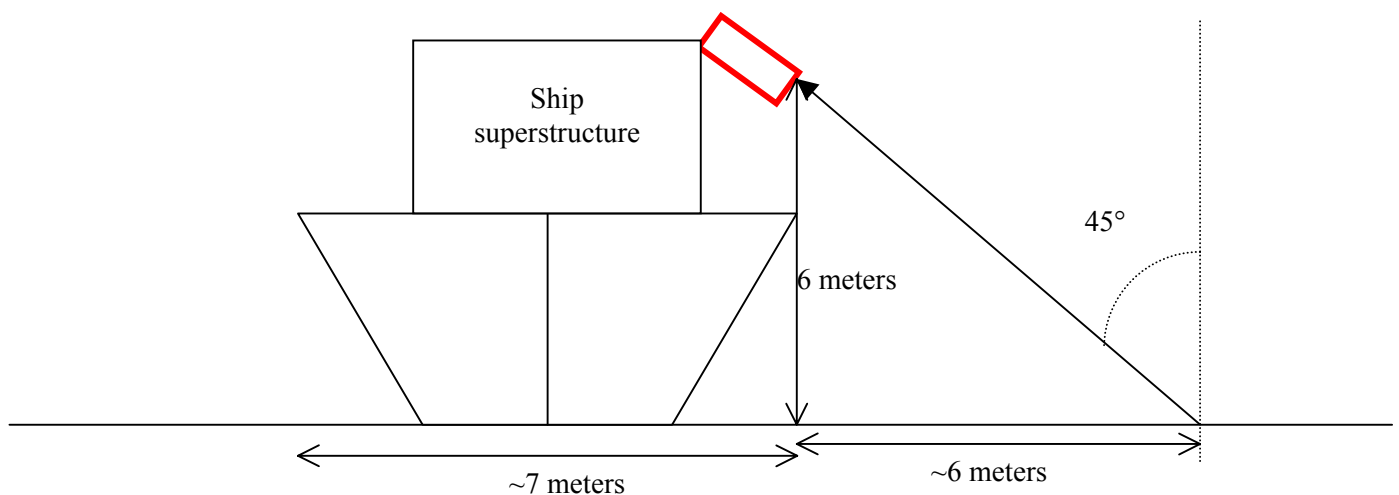
~7 meters

~6 meters

Fig. 5. (cont'd)

Fig. 6. The ship and the two locations from which SIMBADA measurements are performed (green circles)

5   Data processing procedures

5.1   *Processing of the in-water radiometer (SPMR) observations*

It would be out of scope here to go into all details of the data processing procedures that are used for the in-water radiometer observations. The most significant steps are provided when relevant to the problem examined in this report.

5.1.1   *What is measured*

What is measured in the water column is the upwelling irradiance, $E_u(z, \lambda)$ (a summary of all symbols is provided in Appendix 1), at 13 wavelengths from 412 nm to 865 nm (see section 3.1), plus the downwelling irradiance at the same wavelengths, $E_d(z, \lambda)$. The latter is not used in the computation of the reflectance.

The above-water downwelling irradiance $E_d(0^+, \lambda)$ (often referred to as $E_s(\lambda)$), is recorded on deck (at the bow of the ship; Fig. 5), again at the same 13 wavelengths.

5.1.2   *Corrections, extrapolations*

From the vertical profile of $E_u(z, \lambda)$, the upwelling irradiance at null depth ("just below the sea surface") is obtained as (the wavelength, λ, is omitted in the following equations) :

$$E_u(0^-) = E_u(z0) \, e^{(K_u \, z)} \tag{5.1}$$

where z is depth, $E_u(z0)$ is the shallowest value of $E_u(z)$ for which the tilt is lower than 2 degrees, and K_u is the attenuation coefficient for the upwelling irradiance computed from the measurements of $E_u(z)$ collected at all depths between z0 and z0 plus 20 meters.

Several interpolation procedures designed to derive the $E_u(0^-)$ from the vertical profile of $E_u(z)$ have been tested against "true" values of $E_u(0^-)$ (*i.e.*, values directly measured below the sea surface by installing the radiometer on a floating frame), and the method that eventually provided the closest values to the "true" ones was selected.
This experimental work, which is not further detailed here, is just mentioned to indicate that the contribution to the overall error budget of the extrapolation error has been minimised and is below 3% across the entire spectrum.

The above-water reference measurement, $E_d(0^+)$ is corrected to account for the loss of irradiance at the air-sea interface and for the gain of irradiance by internal reflection of the upwelling flux :

$$E_d(0^-) = E_d(0^+) \frac{(1 - \overline{\rho})}{(1 - \overline{r} R)} \tag{5.2}$$

In the above equation, the mean transmission of the sea surface for sky and sun irradiance, expressed by $(1 - \overline{\rho})$, is equal to 0.957 ($\pm$3% according to atmospheric turbidity and sun elevation). The internal reflectance, accounted for by $(1 - \overline{r} R)$, where is $\overline{r} = 0.489$, varies slightly with R. With a mean R value of 3% this term is equal to 0.985 ($\pm$1.5% if R varies between 0 and 6%). We can safely assume that these two terms are constant, so that

$$E_d(0^-) = 0.97 \, E_d(0^+) \tag{5.3}$$

The value of $E_d(0^+)$ that goes into the above equation is obtained from the first 10 seconds of recording starting after the release of the SPMR (this corresponds approximately to the upper 5 meters of the descent), to which a fit is adjusted in order to eliminate variations in $E_d(0^+)$ that are only due to the tilt of the SMSR (which is not installed on a gimbal). This technique provides similar results as compared to just picking the measurements taken for tilt angles < 1°.

5.1.3   *What is eventually computed*

The reflectance R is then computed as :

$$R = E_u(0^-) / \ E_d(0^-) \tag{5.4}$$

Note that before the above ratio is formed, the $E_u(0^-)$ is corrected for instrument self shading as per Gordon and Ding (1992).
In this correction, the instrument radius (*i.e.*, 4.5 cm), the total absorption coefficient (computed following Morel and Maritorena, 2001, and using the measured chlorophyll concentration) and the ratio between direct-sun and diffuse-sky irradiances (computed following Gregg and Carder, 1990) are taken into account.

5.2   *Typical accuracy of reflectance determinations from the SPMR*

Fig. 7 provides one example of the comparison between water-leaving radiances derived from the SPMR[1] and derived from another field radiometer (the "microNESS") that directly measures the upwelling radiance at nadir (so that L_w is straightforwardly obtained as $L_u (1 - \rho) / n^2$).

The unbiased percent differences between both instruments are within 5% in most cases. This is the typical accuracy of in-water determinations of L_w (idem for R) from the SPMR.
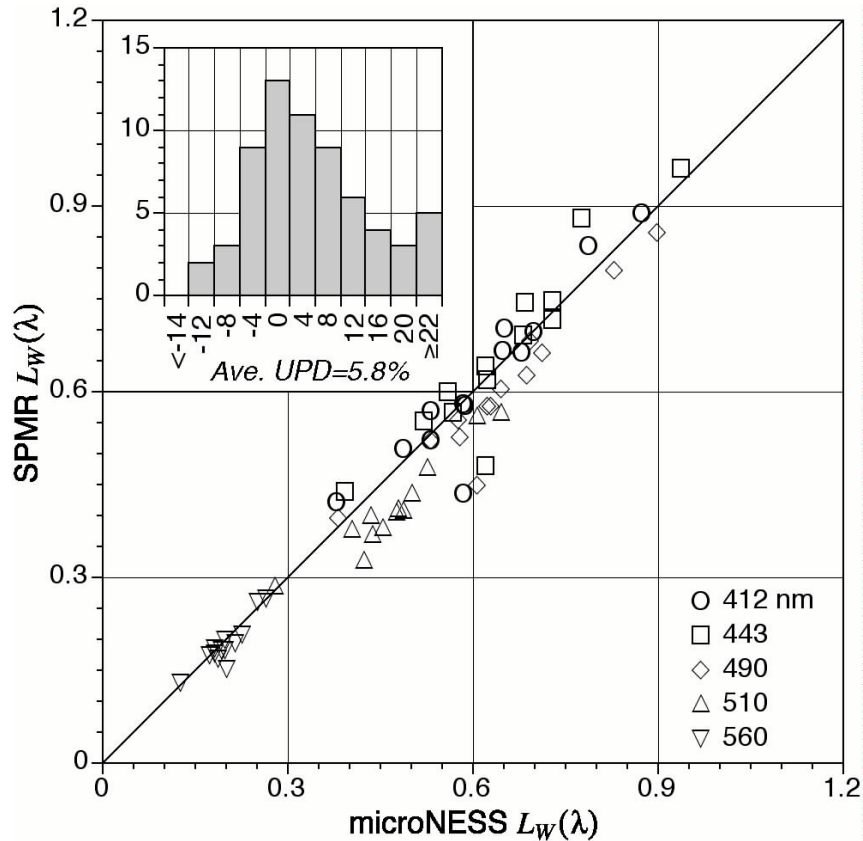
Fig. 7. Comparison between water-leaving radiances obtained with the SPMR (vertical axis) and water-leaving radiances obtained with the microNESS (horizontal axis). Wavelengths are indicated on the figure, and an insert shows the distribution of the unbiased percent differences (UPD = 100 * (x - y) / ((x + y) / 2))). See text for details (figure courtesy Stanford B. Hooker).

The same type of agreement than the one shown in Fig. 7 has been recently obtained between below-water and above-water determinations of the water-leaving radiances (Zibordi *et al.*, 2002). The instruments that were used were a Satlantic's radiometer for the in-water technique and a modified CIMEL sun photometer (scanning the ocean radiance in addition to the sky radiance) for the above-water technique.

5.3   *Processing of the above-water radiometer (SIMBADA) observations*

5.3.1   *A short reminder about "classical" methods for above-water radiometry*

What is measured when aiming at the sea from above the surface is the sum of the water-leaving radiance, generated by backscattering of radiation that have penetrated the ocean interior, of the "sun glint", *i.e.*, direct sun rays reflected back into the instrument field of view by wave facets, and of the "sky glitter", *i.e.*, the reflection from wave facets of diffuse sky radiance into the instrument field of view.

---

[1] R is obtained from the SPMR measurements, and then L_w is computed either as $(E_u / Q) (1 - \rho) / n^2$ or as $E_d(0^+)$ $\mathfrak{R}$ R/Q

A fourth contribution may interplay with the main signals just mentioned, which comes from reflection of sky radiance (or direct sun light in case the instrument is wrongly oriented) from the ship superstructure into the instrument field of view. This perturbation has been found significant (Hooker and Morel, 2003) in case the geometry of the measurement is not carefully maintained.

Let us immediately say that the sun glint can be avoided quite easily by measuring in an appropriate geometry. Residual sun glint, if any, can be eliminated from the measurements by removing any peak in the records.

So, we have (wavelengths omitted) :

$$L_T(\theta_s, [\theta_v, \Delta\phi] \in \Omega) \;=\; L_W(\theta_s, [\theta_v, \Delta\phi] \in \Omega) + \rho_{sea}\, L_{sky}(\theta_s, \Omega') + \rho_{ship}\, L_{sky}(\theta_s, \Omega') \qquad (5.5)$$

where

- ✓ $L_T(\theta_s, [\theta_v, \Delta\phi] \in \Omega)$ is the total radiance measured by the instrument (Ω is the solid angle corresponding to the instrument field of view, including an ensemble of $[\theta_v, \Delta\phi]$ directions),
- ✓ $L_W(\theta_s, [\theta_v, \Delta\phi] \in \Omega)$ is the water-leaving radiance in the same direction, and
- ✓ $L_{sky}(\theta_s, \Omega')$ is the sky radiance for those directions that have been reflected back into the instrument field of view. For a perfectly level surface, Ω' is reduced to the couple ($\pi - \theta_v, \Delta\phi$). As soon as the surface is roughened, Ω' includes an ensemble of directions that is increasingly wide as the wind speed increases (*e.g.*, see Mobley, 1999).
- ✓ ρ_{sea} is an "operational" reflection coefficient, which depends on, but in general does not equal, the Fresnel reflection coefficient. Indeed, ρ_{sea} depends as well on the instrument field of view, wave facets distribution and sky radiance distribution (*e.g.*, see Mobley, 1999).
- ✓ ρ_{ship} is just a convenient way to implicitly merge successive reflections at the sea surface and on the ship superstructure into the instrument field of view. This "coefficient" is a complex function of the geometry during the measurement.

In the following the notation will be simplified as :

$$L_T(\theta_s, \theta_v, \Delta\phi) \;=\; L_W(\theta_s, \theta_v, \Delta\phi) + \rho_{sea}\, L_{sky}(\theta_s, \Omega') + \rho_{ship}\, L_{sky}(\theta_s, \Omega') \qquad (5.6)$$

Neglecting as a first approximation the $\rho_{ship}\, L_{sky}(\theta_s, \Omega')$ contribution, the two usual procedures to estimate $\rho_{sea}\, L_{sky}(\theta_s, \Omega')$ are :

(1) to get a measurement of $L_T(\theta_s, \theta_v, \Delta\phi)$ at a wavelength where $L_W = 0$ (*i.e.*, in the near infrared for Case 1 waters; usually beyond 750 nm), then to form the ratio $L_T(\theta_s, \theta_v, \Delta\phi) / L_{sky}(\theta_s, \Omega')$ at this wavelength, *i.e.*, determining ρ_{sea}, and using this value to compute $\rho_{sea}\, L_{sky}(\theta_s, \Omega')$ at all other wavelengths (Morel, 1980).

(2) Assuming an *a priori* known and constant value for ρ_{sea} and using this value to compute $\rho_{sea}\, L_{sky}(\theta_s, \Omega')$ at all wavelengths (Mueller and Austin, 1995; Mueller *et al*., 2000). In that method, the values of the reflection coefficient are taken from Austin, (1974).

The main difference between the two methods is : procedure number 2 assumes that $\rho_{ship}\, L_{sky}(\theta_s, \Omega')$ is zero, whereas procedure number 1 implicitly includes both $\rho_{sea}\, L_{sky}(\theta_s, \Omega')$ and $\rho_{ship}\, L_{sky}(\theta_s, \Omega')$ when making the measurement of $L_T(\theta_s, \theta_v, \Delta\phi)$ in the near infrared. Using both methods in parallel allows the ship perturbation to be assessed (Hooker and Morel, 2003). Method number 1 cannot apply to Case 2 bright waters where the marine signal is not zero in the near infrared.

Other, more involved, methods have been proposed, which are not further detailed here (*e.g.*, see Lee *et al*., 1997).

5.3.2 *The SIMBADA logic and procedures*

The logic of the SIMBADA processing is different from what has been described above : it is assumed that the $\rho_{\mathrm{sea}}\, L_{\mathrm{sky}}(\theta_{\mathrm{s}}, \Omega')$ contribution is drastically minimised in the measured signal because the instrument is equipped with a vertical polariser and the aiming is performed around the Brewster angle. Indeed, for a flat sea surface, the reflected sky light is fully horizontally polarised, so that it should "disappear" from the measurement performed with the vertical polariser (see a detailed theoretical analysis in Fougnie *et al.*, 1999). Therefore there would be no need for measuring the sky radiance, assuming that the residual perturbation from the sky radiance reflected at the sea surface is very low.

The downwelling irradiance above the sea surface is not measured, and rather it is computed from date and latitude, and by accounting for atmospheric pressure changes (recorded by the ship), ozone concentration (Keating *et al.*, 1989) and the aerosol optical thickness derived from the SIMBADA measurements themselves.

The 5 minima amongst the about 300 recordings (30 to 40 seconds at a 8 Hz frequency) performed by the SIMBADA are averaged, after viewing angles and polariser orientation outside of acceptable limits have been rejected (*i.e.*, instrument roll > 10°, and viewing angles between 40° and 50°). These data are only kept if they are sufficiently homogeneous.

Then the measurements are rejected in case the measured reflectance at 865 nm is larger than 0.004.

A correction is then performed at all wavelengths following :

$$L_T(\theta_{\mathrm{s}}, \theta_{\mathrm{v}}, \Delta\phi) \;=\; L_T(\theta_{\mathrm{s}}, \theta_{\mathrm{v}}, \Delta\phi) - L_g(\theta_{\mathrm{s}}, \theta_{\mathrm{v}}, \Delta\phi) \tag{5.7}$$

where

$$L_g(\theta_{\mathrm{s}}, \theta_{\mathrm{v}}, \Delta\phi) = \frac{L_g(750, \theta_{\mathrm{s}}, \theta_{\mathrm{v}}, \Delta\phi) + L_g(870, \theta_{\mathrm{s}}, \theta_{\mathrm{v}}, \Delta\phi)}{2} \tag{5.8}$$

with

$$L_g(750, \theta_{\mathrm{s}}, \theta_{\mathrm{v}}, \Delta\phi) = L_T(750, \theta_{\mathrm{s}}, \theta_{\mathrm{v}}, \Delta\phi) - \frac{L_T(620, \theta_{\mathrm{s}}, \theta_{\mathrm{v}}, \Delta\phi)}{10}$$

and $\hspace{9cm}$ (5.9)

$$L_g(870, \theta_{\mathrm{s}}, \theta_{\mathrm{v}}, \Delta\phi) = L_T(870, \theta_{\mathrm{s}}, \theta_{\mathrm{v}}, \Delta\phi) - \frac{L_T(670, \theta_{\mathrm{s}}, \theta_{\mathrm{v}}, \Delta\phi)}{10}$$

A last correction is introduced for residual skylight perturbation, which is based on the use of a lookup table, generated from radiative transfer computations. This table contains ???, and is entered into with the viewing angle and the wind speed. It is based on an azimuth difference between the measurement plane and the sun plane of 135°.

The schematic diagram below illustrates the full processing of the SIMBADA data.

Dark file processing

Dark file in

file identification : lat., lon., UT time, …

file processing : mean and std. dev.

dark current output

Sun file processing

Sun file in

file identification : lat., lon., UT time, …

viewing angle calculation

ozone optical thickness correction

molecular optical thickness correction

atmospheric pressure in

3 max. num. counts search for each channel

dark current correction from dark file output

Earth-Sun distance correction

aerosol optical thickness calculation

calibration coefficient in

angstrom coef. and model determination

sun file output

Sea file processing

Sea file in

file identification : lat., lon., UT time, …

viewing angle calculation

optical thickness search from sun file output

zenith and azimut angle sorting algorithm

dark current correction from dark file output

minimum signal search at Brewster angle

total atmospheric transmission calculation

Earth-Sun distance correction

calibration coefficient in

raw reflectance calculation

reflected skylight correction

polarisation correction

4 files synthesis
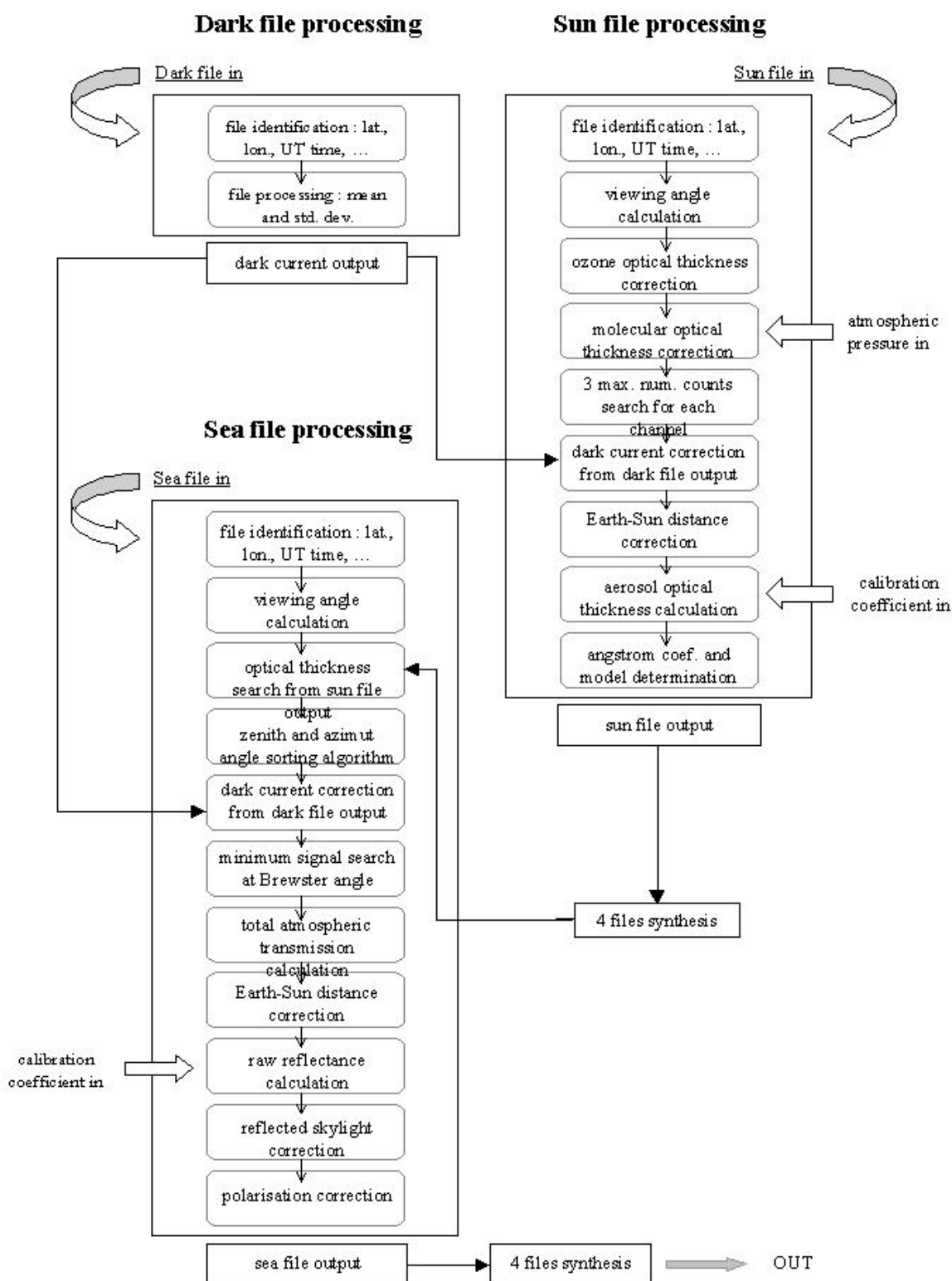
sea file output

4 files synthesis

OUT

Fig. 8. Schematic of the general organisation of the SIMBADA processing code (see at http://www-loa.univ-lille1.fr/recherche/ocean_color/src)

6   The data that have been collected

The table below provides the record of the conditions prevailing during the 121 casts used in the present report. "Sun" and "Vza" stand for the sun zenith angle and the viewing angle (degrees), "AOT" for the aerosol optical thickness at 870 nm, "Eps" for the aerosol Angstrom exponent, and "Chl" for the chlorophyll concentration (mg m^{-3}; determined via HPLC). Cloudiness is provided as okta.

D	M	Y	JJU	H	Lat	Lon	Sun	Hpa	Wind	Octa	O3	AOT	Eps	Vza	Chl
7	22	2001	203	15,305	43,346	7,919	51,660	1027,6	3,10	0	335	0,07263	0,8983	42,6	0,117
7	22	2001	203	15,322	43,346	7,919	51,846	1027,6	3,10	0	335	0,07263	0,8983	44,5	0,117
7	23	2001	204	15,001	43,379	7,921	48,527	1022,3	3,10	2	335	0,15081	1,2659	44,9	0,116
7	23	2001	204	15,250	43,379	7,923	51,205	1022,3	3,10	2	335	0,16085	1,2801	43,1	0,116
7	23	2001	204	15,303	43,379	7,923	51,768	1022,3	3,10	2	335	0,16085	1,2801	44,2	0,116
7	23	2001	204	15,544	43,379	7,927	54,387	1022,3	3,10	2	335	0,17156	1,2895	45,1	0,116
7	24	2001	205	8,407	43,369	7,906	46,063	1037,8	2,60	1	335	0,15819	1,4259	44,3	0,116
7	24	2001	205	8,510	43,370	7,905	44,978	1037,8	2,60	1	335	0,16097	1,4264	43,3	0,116
7	24	2001	205	8,654	43,371	7,905	43,484	1037,8	2,60	1	335	0,16967	1,4019	44,7	0,116
7	24	2001	205	8,795	43,372	7,905	42,040	1035,0	2,37	1	335	0,16567	1,4059	44,9	0,116
7	24	2001	205	8,993	43,372	7,904	40,035	1034,2	2,30	1	335	0,14908	1,4169	43,4	0,116
7	24	2001	205	9,078	43,372	7,903	39,191	1034,5	1,77	1	335	0,14885	1,4235	44,3	0,116
7	24	2001	205	9,254	43,373	7,902	37,468	1032,7	2,30	1	335	0,16083	1,3738	42,7	0,116
7	24	2001	205	11,751	43,368	7,894	23,628	1035,6	2,30	2	335	0,14232	1,278	43,5	0,116
7	24	2001	205	11,833	43,368	7,894	23,742	1034,5	2,63	2	335	0,14148	1,2832	43,7	0,116
7	24	2001	205	12,076	43,370	7,894	24,338	1034,0	2,80	2	335	0,14624	1,2858	43,7	0,116
7	24	2001	205	12,325	43,372	7,894	25,321	1035,1	2,00	2	335	0,14921	1,3285	44,6	0,116
7	24	2001	205	12,427	43,372	7,893	25,818	1035,1	2,00	2	335	0,15288	1,3176	44,1	0,116
9	2	2001	245	8,270	43,357	7,884	54,851	1001,3	3,09	0	307	0,0538	0,3011	45,7	0,065
9	2	2001	245	8,580	43,354	7,877	51,865	1001,3	3,09	0	307	0,05971	0,307	44,7	0,065
9	2	2001	245	8,850	43,352	7,871	49,379	1006,9	2,06	0	307	0,05777	0,303	44,9	0,065
9	2	2001	245	9,134	43,349	7,863	46,890	1008,7	2,06	0	307	0,0581	0,3256	45,6	0,065
9	2	2001	245	9,613	43,347	7,850	43,074	1011,6	2,06	0	307	0,06084	0,2255	47,5	0,065
9	2	2001	245	9,873	43,346	7,843	41,243	1011,6	2,06	0	307	0,05998	0,2511	48,4	0,065
9	3	2001	246	8,960	43,377	7,911	48,626	1004,2	6,17	0	307	0,05439	0,6975	43,9	0,077
9	3	2001	246	9,193	43,383	7,917	46,636	1004,2	6,17	0	307	0,05695	0,6841	42,5	0,077
9	3	2001	246	9,482	43,391	7,925	44,328	1004,2	6,17	0	307	0,05748	0,6816	46,7	0,077
9	3	2001	246	9,716	43,397	7,933	42,604	1004,2	6,17	0	307	0,05814	0,6773	44,7	0,077
9	3	2001	246	12,097	43,368	7,897	36,847	1004,2	6,17	0	307	0,05826	0,3708	45,1	0,095
9	3	2001	246	12,113	43,368	7,898	36,892	1004,2	6,17	0	307	0,05826	0,3708	44,8	0,095
9	3	2001	246	12,520	43,370	7,895	38,491	1004,3	6,17	0	307	0,06105	0,481	43,2	0,095
9	3	2001	246	12,708	43,369	7,901	39,450	1004,3	6,17	0	307	0,05946	0,4822	45,0	0,095
9	3	2001	246	13,064	43,371	7,880	41,594	1004,2	6,17	0	307	0,05786	0,3897	45,5	0,095
9	3	2001	246	13,278	43,368	7,885	43,079	1005,0	6,17	0	307	0,05627	0,3092	44,1	0,095
9	3	2001	246	13,357	43,367	7,887	43,662	1005,0	6,17	0	307	0,05582	0,2793	45,4	0,095
3	24	2002	83	13,471	43,612	7,326	48,794	1019,0	5,66	0	401	0,05658	1,2614	45,4	0,203
3	24	2002	83	13,561	43,613	7,325	49,409	1019,0	5,66	0	401	0,05772	1,2242	46,5	0,203
3	24	2002	83	13,688	43,615	7,323	50,314	1019,0	5,66	0	401	0,05831	1,2428	44,9	0,203
3	24	2002	83	13,820	43,617	7,322	51,292	1019,0	5,66	1	401	0,06025	1,2471	48,5	0,203
3	24	2002	83	14,019	43,619	7,320	52,844	1019,0	5,66	1	401	0,06293	1,276	47,2	0,203
3	24	2002	83	14,655	43,609	7,330	58,301	1019,0	5,66	1	401	0,07643	1,2372	46,1	0,203
5	20	2002	140	12,865	43,370	7,899	29,632	1013,3	3,09	0	382	0,11581	1,3065	45,6	0,106
5	20	2002	140	13,107	43,370	7,902	31,582	1013,3	3,09	0	382	0,11322	1,3361	44,9	0,106
5	20	2002	140	14,539	43,374	7,903	45,448	1013,0	3,09	1	382	0,11644	1,3744	45,5	0,106
6	27	2002	178	11,617	43,384	7,888	20,087	1016,5	4,00	1	360	0,24598	1,0072	44,8	0,103
6	27	2002	178	12,393	43,372	7,895	22,760	1016,5	4,00	1	360	0,28557	0,9037	44,5	0,103
6	28	2002	179	9,396	43,582	7,530	33,387	1008,1	11,00	0	360	0,14949	1,291	45,4	0,064
6	28	2002	179	10,315	43,576	7,504	25,387	1007,6	2,00	0	360	0,12504	1,2146	44,9	0,064
6	28	2002	179	10,326	43,576	7,504	25,304	1007,6	2,00	0	360	0,12504	1,2146	45,6	0,064
7	20	2002	201	14,369	43,366	7,899	41,510	1016,5	0,90	2	335	0,15679	1,535	45,6	0,114
7	20	2002	201	15,075	43,367	7,898	48,948	1016,5	0,90	1	335	0,2263	1,2674	45,2	0,114
7	20	2002	201	16,709	43,366	7,896	66,685	1016,5	0,90	2	335	0,17303	1,6564	45,7	0,114
7	21	2002	202	11,953	43,373	7,891	23,399	1016,7	4,40	2	335	0,19021	1,0145	45,7	0,111
7	21	2002	202	12,823	43,368	7,904	27,717	1016,7	4,40	2	335	0,19994	0,845	45,7	0,111
7	21	2002	202	14,536	43,371	7,902	43,356	1016,7	2,50	2	335	0,26738	0,4564	46,1	0,111
7	21	2002	202	15,542	43,376	7,916	54,110	1016,7	2,50	2	335	0,24373	0,4491	45,2	0,111
7	21	2002	202	16,427	43,381	7,927	63,765	1016,7	2,50	2	335	0,25759	0,3565	44,7	0,111
7	22	2002	203	5,466	43,367	7,905	77,458	1016,7	0,90	2	335	0,1569	1,3249	46,2	0,157
7	22	2002	203	6,602	43,360	7,905	65,299	1016,7	0,90	2	335	0,17127	1,247	45,0	0,157
7	22	2002	203	7,534	43,363	7,900	55,151	1016,7	0,90	2	335	0,15127	1,2607	44,9	0,157

D	M	Y	JJU	H	Lat	Lon	Sun	Hpa	Wind	Octa	O3	AOT	Eps	Vza	Chl
7	22	2002	203	8,268	43,362	7,900	47,252	1016,7	0,90	2	335	0,14572	1,0957	45,3	0,157
7	22	2002	203	11,424	43,356	7,894	23,194	1016,7	0,00	1	335	0,12121	1,3361	45,3	0,157
9	3	2002	246	14,300	43,372	7,891	51,654	1019,9	2,50	1	307	0,12934	1,6271	45,8	0,12
9	3	2002	246	15,850	43,367	7,899	67,373	1018,0	2,50	1	307	0,11329	1,661	45,6	0,12
10	5	2002	278	9,661	43,364	7,897	52,885	1020,0	1,54	2	302	0,12287	1,6473	47,5	0,177
10	5	2002	278	9,852	43,363	7,898	51,869	1020,0	1,54	2	302	0,11289	1,653	47,5	0,177
10	5	2002	278	10,037	43,362	7,896	50,993	1020,0	1,54	2	302	0,1103	1,6537	46,4	0,177
3	17	2003	76	10,788	43,543	7,747	46,202	1027,9	6,17	0	401	0,04927	1,6062	47,0	0,55
3	17	2003	76	10,819	43,543	7,747	46,101	1027,9	6,17	0	401	0,04927	1,6062	48,9	0,55
3	17	2003	76	12,634	43,527	7,746	46,770	1027,0	5,14	0	401	0,04144	1,338	49,1	0,55
3	17	2003	76	12,663	43,526	7,746	46,885	1027,0	5,14	0	401	0,04144	1,338	49,0	0,55
5	28	2003	148	7,371	43,369	7,888	54,440	1014,8	2,57	0	382	0,28389	1,4081	45,8	0,158
5	28	2003	148	7,911	43,363	7,900	48,575	1014,8	2,06	0	382	0,27381	1,3688	46,5	0,158
5	28	2003	148	8,117	43,364	7,895	46,368	1014,9	3,09	0	382	0,26627	1,3868	47,5	0,158
5	28	2003	148	8,306	43,364	7,891	44,365	1014,9	3,09	0	382	0,2567	1,4209	47,1	0,158
5	28	2003	148	9,053	43,364	7,899	36,689	1014,9	3,09	0	382	0,22581	1,3695	46,1	0,158
5	28	2003	148	9,307	43,364	7,894	34,228	1014,9	3,09	0	382	0,22581	1,3695	46,6	0,158
5	28	2003	148	12,481	43,370	7,900	25,543	1014,4	2,06	0	382	0,37947	0,8465	46,1	0,142
5	28	2003	148	13,496	43,367	7,903	33,808	1013,9	2,06	0	382	0,1709	1,2703	46,3	0,142
5	28	2003	148	13,757	43,369	7,906	36,325	1013,9	2,06	0	382	0,1709	1,2703	46,5	0,142
5	28	2003	148	14,538	43,365	7,903	44,331	1013,1	4,12	0	382	0,15156	1,3053	47,1	0,142
5	29	2003	149	7,780	43,362	7,901	49,912	1012,9	1,03	0	382	0,14913	1,4318	46,4	0,16
5	29	2003	149	7,996	43,359	7,901	47,588	1012,8	1,03	0	382	0,15075	1,4102	47,4	0,16
5	29	2003	149	9,311	43,359	7,900	34,092	1013,0	0,51	0	382	0,14788	1,3073	46,6	0,16
5	29	2003	149	9,469	43,357	7,897	32,613	1013,0	0,51	0	382	0,14806	1,3061	48,1	0,16
5	29	2003	149	9,572	43,356	7,897	31,672	1013,0	0,51	0	382	0,14786	1,3068	47,6	0,16
5	29	2003	149	11,079	43,364	7,897	22,139	1012,9	2,06	0	382	0,14266	1,1958	47,9	0,16
5	29	2003	149	11,362	43,362	7,890	21,724	1012,6	2,06	0	382	0,14212	1,2015	47,2	0,16
6	27	2003	178	8,978	43,367	7,900	37,165	1010,9	1,03	0	360	0,38565	1,0147	45,6	0,085
6	27	2003	178	9,113	43,366	7,902	35,786	1010,9	1,03	0	360	0,38565	1,0147	45,5	0,085
6	27	2003	178	12,245	43,369	7,901	21,951	1010,4	3,09	1	360	0,3834	1,0512	47,5	0,085
6	27	2003	178	12,677	43,374	7,897	24,619	1010,5	2,06	1	360	0,38231	1,0211	48,0	0,085
6	27	2003	178	14,171	43,368	7,898	38,264	1010,1	3,60	1	360	0,52784	0,6905	48,2	0,085
6	27	2003	178	14,362	43,371	7,897	40,252	1010,1	3,60	1	360	0,52784	0,6905	48,8	0,085
6	28	2003	179	16,146	43,367	7,897	59,523	1009,7	0,51	2	-100	-1	-9,9	47,4	0,077
6	29	2003	180	11,158	43,365	7,899	20,643	1010,9	4,12	0	360	0,19831	1,1818	45,7	0,093
6	29	2003	180	12,965	43,365	7,892	26,851	1010,9	2,57	0	360	0,20167	1,1309	47,5	0,093
6	29	2003	180	12,985	43,365	7,892	27,013	1010,9	2,57	0	360	0,19747	1,1571	47,2	0,093
6	29	2003	180	15,394	43,369	7,899	51,322	1010,3	1,54	0	360	0,17924	1,2479	46,7	0,093
6	29	2003	180	15,416	43,369	7,898	51,556	1010,3	1,54	0	360	0,17924	1,2479	44,8	0,093
7	13	2003	194	13,154	43,365	7,899	29,223	1013,5	1,54	1	335	0,22139	1,4901	46,2	0,066
7	13	2003	194	13,371	43,368	7,901	31,104	1013,4	1,54	1	335	0,23084	1,4738	46,7	0,066
7	13	2003	194	13,581	43,371	7,902	33,024	1013,4	2,57	1	335	0,22972	1,4621	46,6	0,066
7	13	2003	194	13,770	43,372	7,903	34,819	1013,4	2,57	1	335	0,22877	1,4555	46,2	0,066
7	14	2003	195	8,649	43,368	7,900	42,182	1012,4	4,12	0	335	0,2523	1,5668	47,9	0,083
7	14	2003	195	8,885	43,366	7,896	39,737	1012,5	4,12	0	335	0,23407	1,5533	46,2	0,083
7	14	2003	195	9,087	43,365	7,892	37,690	1012,5	4,12	0	335	0,22951	1,543	46,5	0,083
7	14	2003	195	9,269	43,364	7,888	35,891	1012,5	4,12	0	335	0,22511	1,5368	46,8	0,083
7	14	2003	195	11,311	43,370	7,887	21,945	1012,3	3,09	0	335	0,24531	1,4542	46,1	0,06
7	14	2003	195	11,322	43,370	7,887	21,926	1012,3	3,09	0	335	0,24885	1,4547	45,8	0,06
7	14	2003	195	11,603	43,372	7,881	21,711	1012,2	3,60	0	335	0,25984	1,4599	46,2	0,06
7	14	2003	195	11,883	43,373	7,875	22,056	1012,2	3,60	0	335	0,26383	1,4629	46,2	0,06
7	14	2003	195	12,959	43,369	7,896	27,758	1012,1	2,57	0	335	0,26432	1,4807	46,6	0,06
7	14	2003	195	13,160	43,371	7,892	29,380	1012,1	2,37	0	335	0,26066	1,4743	46,9	0,06
7	14	2003	195	13,352	43,372	7,888	31,026	1012,0	2,06	0	335	0,25069	1,4708	47,6	0,06
7	14	2003	195	13,720	43,378	7,883	34,423	1012,0	2,06	0	335	0,25087	1,4774	47,4	0,06
7	15	2003	196	10,108	43,364	7,894	28,469	1013,0	6,17	0	335	0,2199	1,1952	46,2	0,07
7	15	2003	196	10,366	43,363	7,885	26,536	1013,0	6,17	0	335	0,21908	1,1918	49,7	0,07
7	15	2003	196	10,500	43,362	7,881	25,628	1013,0	6,17	0	335	0,22128	1,1898	47,1	0,07
7	15	2003	196	11,956	43,368	7,895	22,379	1012,9	4,12	0	335	0,1998	1,1387	44,8	0,07
7	15	2003	196	11,966	43,368	7,895	22,406	1012,9	4,12	0	335	0,1998	1,1387	49,6	0,07

7   Inter-comparison results

7.1   Relationships between above-water and in-water radiometric quantities

The SIMBADA radiometer is measuring directly a radiance in a given viewing direction θ_v, which corresponds to an underwater nadir angle θ'. This radiance is a water-leaving radiance, as far as the contribution of reflection at the sea surface has been removed. This water-leaving radiance can be expressed as (*e.g.*, Morel and Gentili 1996) :

$$L_w(\theta_s,\theta_v,\Delta\phi) = E_d(0^+)\,\Re(\theta')\,\frac{f(\theta_s)}{Q(\theta_s,\theta',\Delta\phi)}\,f(IOP) = \left(\varepsilon_c\,F_0\,\mu_s\,t_d(\theta_s)\right)\Re(\theta')\,\frac{f(\theta_s)}{Q(\theta_s,\theta',\Delta\phi)}\,f(IOP) \quad (7.1)$$

where f(IOP) is a given function of the inherent optical properties (IOPs), often taken as the ratio of the backscattering coefficient to the absorption coefficient.

The angle θ' is the viewing angle below the surface ($\theta' = \sin^{-1}(\sin(\theta_v)\,/\,1.34)$), and the gothic R ($\Re$) is a factor accounting for all reflection and transmission effects at the air-sea interface. It is equal to (subscript 0 when $\theta' = 0$) :

$$\Re(\theta') = \left[\frac{(1-\overline{\rho})}{(1-\overline{r}\,R)}\,\frac{(1-\rho_F(\theta'))}{n^2}\right] \quad (7.2)$$

where n is the refractive index of water, $\rho_F(\theta)$ is the Fresnel reflection coefficient for incident angle θ, $\overline{\rho}$ is the mean reflection coefficient for the downwelling irradiance at the sea surface, and $\overline{r}$ is the average reflection for upwelling irradiance at the water-air interface. The reflectance that is provided by the LOA-SIMBADA project is equal to :

$$\rho_{simb}(\theta_s) = \pi\,L_w(\theta_s,\theta_v,\Delta\phi)\,/\,E_d(0^+) \quad (7.3)$$

or, equivalently, to (see Eqs. 7.1 and 7.2) :

$$\rho_{simb}(\theta_s) = \pi\,\Re(\theta')\,\frac{f(\theta_s)}{Q(\theta_s,\theta',\Delta\phi)}\,f(IOP) \quad (7.4)$$

The symbol ρ is used to express that this is a "directional reflectance".

The LOV SPMR radiometer is providing the above-surface downwelling irradiance and the below-water upwelling and downwelling irradiances. The irradiance reflectance R that is derived from these measurements (see section 5.1) is expressed as :

$$R_{spmr}(\theta_s) = f(\theta_s)\,f(IOP) \quad (7.5)$$

The relationship between both reflectances is therefore :

$$R_{simbada}(\theta_s) = \frac{\rho_{simb}(\theta_s)\;\;Q(\theta_s,\theta',\Delta\phi)}{\pi\;\;\Re(\theta')} \quad (7.6)$$

which is simply the combination of a geometrical correction and of corrections needed between above-water and below-water measurements.

In this transformation, the Q factor is needed to account for the fact that the SIMBADA aims at a non-isotropic reflectance at an angle of about 40°, and the "gothic R" is needed to incorporate the

transmission / refraction effects at the sea surface, which intervene in this comparison between an above-water and a below-water techniques. Note that both measurements (SPMR and SIMBADA) are taken either simultaneously or at a very small time interval (5 to 10 minutes maximum), so that changes in solar elevation are negligible.

The Q factors recently revised by Morel *et al.* (2002) have been used here, with the relevant geometry (solar elevation, viewing angle and azimuth difference between the sun and the SIMBADA aiming), and by using the chlorophyll concentration as measured (HPLC) from filtered samples taken on site between the optics casts.

What we did as well was to use the downwelling irradiance as measured by the SMSR (*i.e.*, the deck reference sensor used in parallel to the SPMR) to re-compute the SIMBADA reflectances, instead of using the calculated value of the downwelling irradiance. By this way, we have on the one hand a full compatibility in terms of the above-surface reference downwelling irradiance, and, on the other hand, we have a mean to eliminate situations for which the difference between the computed and the calculated surface irradiances is larger than 5% (which was only occurring for less than 10% of the stations). This is a check that the SIMBADA was used in truly clear sky conditions.

Some situations are shown on Fig. 9, where the computed (red curve) and measured $E_d(0^+)$ (black curve) spectra are shown, as well as the relative percent difference between both.

The full transformation needed to express the SIMBADA measurement in terms of R is therefore :

$$R_{simbada}(\theta_s) = \frac{\rho_{simb}(\theta_s)}{\pi} \frac{Q(\theta_s, \theta', \Delta\phi)}{\Re(\theta')} \frac{E_d(0^+)_{SIMBADA}}{E_d(0^+)_{SPMR}} \tag{7.7}$$

7.2   Results

7.2.1   Reflectances

All matchup points, *i.e.*, all stations and all wavelengths, have been pooled together to draw a general matchup plot of the SIMBADA-derived reflectances *versus* the SPMR-derived reflectances (Fig. 10a). This is shown both with linear axes and in a log-log space. The latter is necessary to distinguish amongst the different wavelengths in the red part of the visible spectrum.

The data are plotted with different symbols as a function of the value of the sun zenith angle : diamonds for solar zenith angles between 20° and 30°, circles for values between 30° and 40°, squares between 40° and 50°, triangles between 50° and 60°, and stars above 60°.

The colours are used to distinguish between wavelengths : black is 412 nm, deep blue is 443 nm, light blue is 490 nm, dark green is 510 nm, light green is 560 nm, red is 620 nm and pink is 665 nm.

The insert on the lower corner of the figure provides for each wavelength the values of the absolute differences (x – y), bias 100. * ((x – y) / x) and unbiased percent difference 100. * ((x – y) / [(x + y) / 2]) between the SIMBADA and the SPMR reflectances. These three different measures of the differences between the two reflectance sets are provided on Figs. 11, 12 and 13, as histograms (one histogram per wavelength). Individual reflectance spectra are provided in Appendix 2.

The coefficient of regression and the slope and intercept of a linear regression are also displayed on Fig. 10a.

There is an overall overestimation of the SIMBADA reflectance as compared to the SPMR reflectance, with a slope of the linear regression between both equal to 1.13 and a large intercept of 0.0017. Considering the mean values of the reflectance in different parts of the spectrum, these numbers means a factor of 2 around 620 nm between the SIMBADA and the SPMR, and an average 15% overestimation by the SIMBADA in the blue.

The dispersion of the points is large, with root mean square differences (RMSD) of 15.2% at 412 nm, 17.6% at 443 nm, 28.4% at 490 nm, 22% at 510 nm, 36.4% at 560 nm, 93% at 620 nm and 174% at 670 nm. These RMSD were computed as

$$RMSD = \sqrt{\frac{1}{N} \sum_{1}^{N} \left(1 - \frac{R_{simbada}}{R_{spmr}} \right)^2} \qquad (7.8)$$

The bias is from about 14% at 412 nm to about 30% at 490 and 560 nm. In the red, the marine signal is low for oligotrophic to mesotrophic waters, so that errors rapidly exceed the signal itself, leading to relative differences between both measurement types larger than 100%.

In order to investigate the possible impact of inaccurate Q factors, we have applied Eq. (6.7) by using values of 45, 90 and 180 degrees instead of the nominal 135 degrees for the azimuth angle between the vertical plane of the measurements and the vertical plane containing the sun. The differences are of a few percents and do not substantially reduce neither the bias (it is even increased for $\Delta\phi = 45°$) nor the scatter observed on Fig. 10.

This result was expectable since the range of chlorophyll concentration for which the comparisons have been performed (*i.e.*, 0.05 to 0.2 mg m^{-3}) is the range where the Q factors are the less uncertain (*e.g.*, see Morel *et al.*, 1995). Therefore the uncertainty that persists on the exact values of the Q factors cannot be invoked to explain the observed differences.

7.2.2   *Band ratios*

Water-leaving reflectances are usually combined through band ratio algorithms, which are supposed to provide a geophysical quantity from this ratio, usually the chlorophyll concentration (*e.g.*, see O'Reilly *et al.*, 2001).

Therefore we have plotted (Fig. 14) the 443/560 nm and the 490/560 nm band ratios, as derived either from the SPMR reflectances or from the SIMBADA reflectances. As expected from the dispersion of the results for individual wavelengths (Fig. 10), the ratio are not well correlated. They differ on average by 0.5.

The resulting differences in terms of the chlorophyll concentration would be between around a factor of 2, in the direction of an underestimate of the chlorophyll concentration, since the blue-to-green ratio would be overestimated.

7.2.3   *Tentative residual sky light correction*

The fact that the absolute differences between the SIMBADA and the SPMR measurements are increasing from the red to the blue suggests that they might be due to a residual contamination of the SIMBADA measurements by some skylight reflected at the sea surface. This sky radiance has indeed a strong spectral dependence.

A purely empirical correction has been accordingly tested, where a residual sky light contribution, $L_{sky,residual}$, is removed from the SIMBADA measurements. This contribution is computed as :

$$L_{sky,residual} \;\; = \;\; \rho_{sea}\, L_{sky}(\theta_s, \Omega')\, C_{residual} \qquad (7.9)$$

where L_{sky} is computed using a radiative transfer code, for a molecular atmosphere and a standard atmospheric pressure of 1013 hPa.

It has been found that a better fit between the SIMBADA and the SPMR reflectances was obtained when the coefficient $C_{residual}$ in Eq. (7.9) was set to 0.7 (ρ_{sea} being equal to 2.8%; Austin, 1974). This very large coefficient would indicate that elimination of the reflected sky radiance by means of the polariser is insufficient (more or less 50% to 70% of the reflected sky light would still enter the instrument). It should be kept in mind that the theoretical study of Fougnie *et al.* (1999) indicated that the substantial reduction of reflected skylight near the Brewster angle becomes nil at a viewing angle of 30 degrees, indicating how important it is to follow the measurement protocol.

The results are shown on Figs 10(b), 15 (to be compared with Fig. 11), 16 (12), 17 (13) and 18 (14). The dispersion of the points is obviously not affected by this spectrally-smooth correction, yet the biases are substantially reduced (for instance from 14% to nearly 0 at 412 nm and from 30% to 15% at 490 nm).

Using the actual values of the atmospheric pressure and computing the sky radiance for a realistic atmosphere containing aerosols would probably be more relevant, and would probably again improve a

bit the comparison (in that case it could also reduce the scatter). These refinements have not been tested, however. The aim of using Eq. (7.9) is indeed just to quantify the overestimation of the reflectances by the SIMBADA and to provide a possible clue for it.

Although the reason for the discrepancy between the SPMR and the SIMBADA measurements has perhaps nothing to do with a residual, uncorrected, sky radiance (*e.g.*, calibration, instrument field of view characterisation, correction to derive the water-leaving radiance from its polarised value …), the present exercise provides a measure of the correction that is needed to reconcile the reflectance determinations by both radiometers. It is of the order of half the reflected sky radiance. Clearly the differences observed here cannot be entirely due to the inherent differences between the two techniques, *i.e.*, above and below water techniques. Other reasons necessarily exist, which have not been identified in this study.

8   Conclusions & recommendations

The comparison performed here between above-water (SIMBADA instrument) and in-water (SPMR/SMSR instrument) determinations of the ocean reflectance is not fully satisfactory. The reason for the observed differences are not clearly identified (what is presented in section 7.2.3 is just tentative). Resolving these discrepancies would probably require dedicated experiments involving several types of above-water and in-water instruments. As an example, we show here the comparison between SIMABA-derived reflectances and reflectances obtained from other above-water systems, *i.e.*, the microSAS and SunSAS (Fig. 19). The bias is again of about 15% with the reflectances derived from the SIMBADA being larger than the values derived from the other techniques (and up to ~25% in the blue).

The bias and RMS between both estimates is larger than the 5% accuracy which is aimed at when collecting reflectance measurements at sea in view of the validation of ocean colour satellite-borne sensors (*cf.* section 1 of this report).

Possible improvements of the protocol can be suggested, that might help in reconciling the SIMBADA measurements with the measurements of in-water instruments.

They are as follows :

✓ Having parallel measurements without polarisation at one or two wavelengths, in order to check the efficiency of the polariser; in case the RefPol instrument is still available (Fougnie *et al.*, 1999), it could be useful for that purpose. The same results could be obtained with the use of another above-water system for the determination of the reflectance.
✓ Recording $E_d(0^+)$: even if computed and measured values were within 5% in most case, this is not systematic and introduces an additional uncertainty, larger than the calibration uncertainty in the measurement of $E_d(0^+)$.
✓ Being more restrictive when eliminating non-zero roll angles, *i.e.*, keeping only measurements for which the angles are close to the theoretical configuration where elimination of the sky light indeed occurs.
✓ Taking note of more environmental parameters such as the exact orientation of the measurement from the sun azimuth, the height above the water (hence the distance of the pixel from the ship hull), the swell orientation (if any).
✓ Making longer recordings (total 1 minute, so at least 6 times the 11-second sequence that is pre-programmed in the SIMBADA), in order to increase the chances to get minimum values (no glint contamination) and relevant geometrical configurations.

This type of changes in the protocol would imply that the instrument is operated by a well-trained user, and that a maximum of information are recorded about the environmental conditions prevailing during the measurement sequences.

This would be useful for helping in the process of selecting good data among the whole set of measurements, as well as further understanding the response of the SIMBADA radiometer in various sea conditions.

9   Acknowledgements

10   References

Austin R.W. , 1974, The remote sensing of spectral radiance from below the ocean surface," in *Optical Aspects of Oceanograph*y, N. G. Jerlov and E. S. Nielsen, eds. Academic, San Diego, Calif., 317–344.

Fougnie B., R. Frouin, P. Lecomte and P.-Y. Deschamps, 1999, Reduction of skylight reflection effects in the above-water measurement of diffuse marine reflectance. *Applied Optics* **38(18)**, 3844-3856.

Gordon H.R. and Ding, 1992, Self-shading of in-water optical instruments, *Limnology and Oceanography* **37**, 491-500.

Gregg W.W. and K.L. Carder, 1990, A simple spectral solar irradiance model for cloudless maritime atmospheres. *Limnology and Oceanography* **35**, 1657-1675.

Hooker S.B. and J.A. Aiken, 1998, Calibration evaluation and radiometric testing of field radiometers with the SeaWiFS quality monitor (SQM), *Journal of Atmospheric and Oceanic Technology* **15**, 995-1007.

Hooker S.B., G. Lazin, G. Zibordi and S. McLean, 2002, An evaluation of above- and in-water methods for determining water-leaving radiances, *Journal of Atmospheric and Oceanic Technology* **19**, 486-515.

Hooker S.B. and A. Morel, 2003, Platform and environmental effects on above-water determinations of water-leaving radiances, *Journal of Atmospheric and Oceanic Technology* **20**, 187-205.

Keating et al., 1989, Ozone reference models for the middle atmosphere in Handbook for MAP, Vol. 31.

Lee Z.P., K.L. Carder, R.G. Steward, T.G. Peacock, C.O. Davis and J.L. Mueller, 1997, Remote-sensing reflectance and inherent optical properties of oceanic waters derived from above-water measurements, in *Ocean Optics XIII*, S.G. Ackleson and R. Frouin Eds., *Proc. SPIE* **2963**, 160-166.

Mobley C.D., 1999, Estimation of the remote-sensing reflectance from above-surface measurements, *Applied Optics* **38**, 7442-7455.

Morel A., 1980, In-water and remote measurements of ocean colour. *Boundary-layer Meteorology* **18**, 177-201.

Morel, A., Antoine, D. and B. Gentili, 2002, Bidirectional reflectance of oceanic waters: Accounting for Raman emission and varying particle phase function, *Appied Optics* **41**, 6289-6306.

Morel, A., and Gentili, B., 1993, Diffuse reflectance of oceanic waters. II. Bidirectional aspects, *Applied Optics* **32**, 6864-6879.

Morel, A., and Gentili, B., 1996, Diffuse reflectance of oceanic waters. III. implication of the bidirectionality for the remote sensing problem, *Applied Optics* **35**, 4850-4862.

Morel, A., and S. Maritorena, 2001, Bio-optical properties of oceanic waters: A reappraisal. *Journal of Geophysical research* **106**, 7763-7780.

Morel, A., Voss, K.J. and B. Gentili, 1995, Bidirectional reflectance of oceanic waters: A comparison of modeled and measured upward radiance fields, *Journal of Geophysical Research* **100**, 13,143-13,150.

Mueller J.L., and R.W. Austin, 1995, Ocean Optics Protocols for SeaWiFS validation, rev. 1, NASA Tech. Memo 104566, Vol. 25, S.B. Hooker and E.R. Firestone Eds., NASA GSFC, Maryland, 43 pp.

O'Reilly, J.E., Maritorena, S., Mitchell, B.G., Siegel, D.A., Carder, K.L., Garver, S.A., Kahru, M. and McClain, C., 1998, Ocean color chlorophyll algorithms for SeaWiFS. *Journal of Geophysical Research* **103**, 24,937-24,953.

Toole D.A., D.A. Siegel, D.W. Menzies, M.J. Neumann and R.C. Smith, 2000, Remote-sensing reflectance determinations in the coastal ocean environment : impact of instrumental characteristics and environmental variability, *Applied Optics* **39(3)**, 456-469.

Zibordi G., S.B. Hooker, J.F. Berthon and D. D'Alimonte, 2002, Autonomous above-water radiance measurements from an offshore platform : a field assessment experiment, *Journal of Atmospheric and Oceanic Technology* **19**, 808-819.
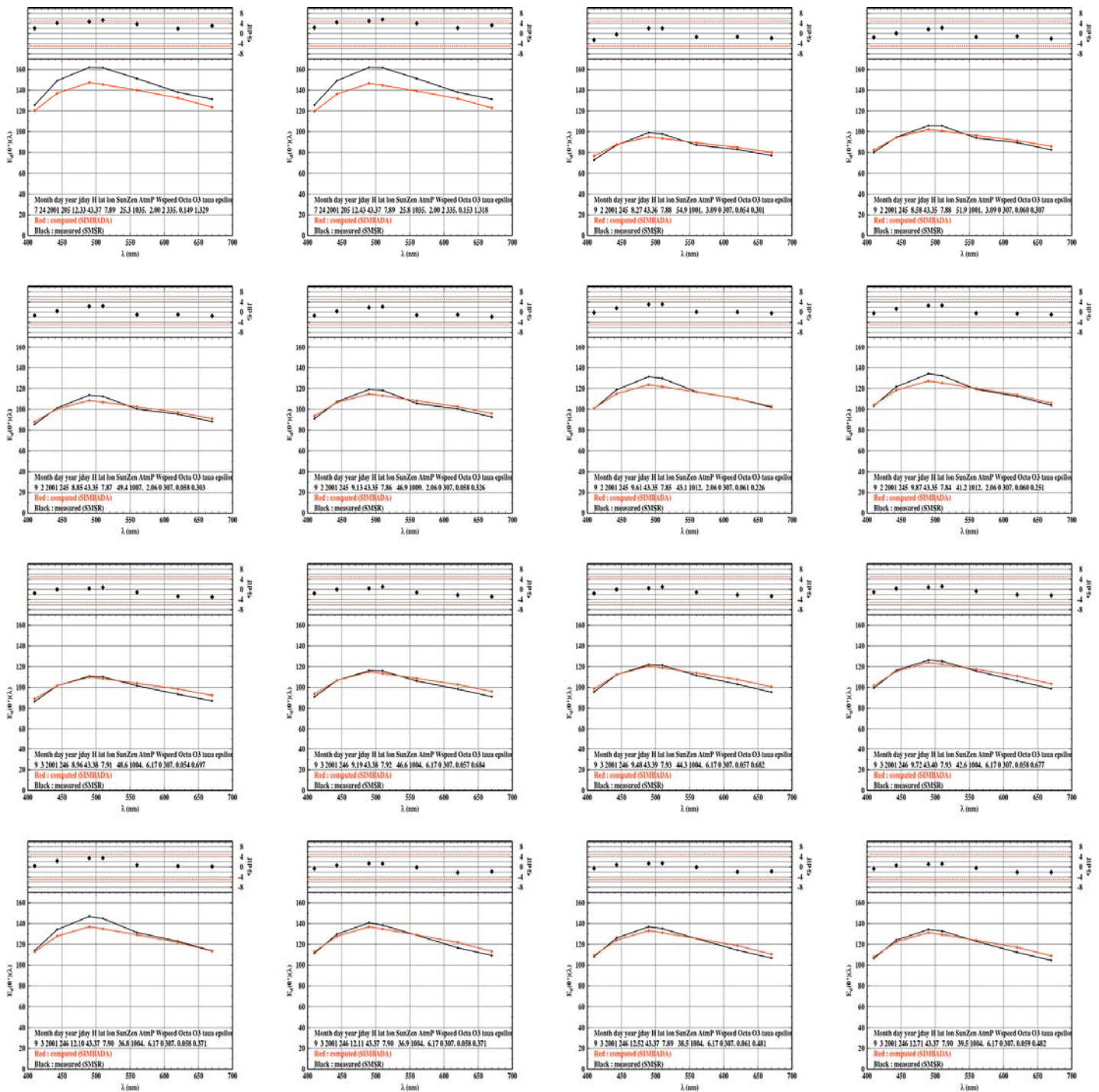
Fig. 9. Examples of the downwelling irradiance measured just above the sea surface with the SMSR (black curves) and computed through the SIMBADA processing for the same level and using the aerosol optical thickness determined from the SIMBADA measurements themselves (atmospheric pressure is taken from the ship meteo record). The relative difference between both is shown on top of each panel (red lines for ±5%).
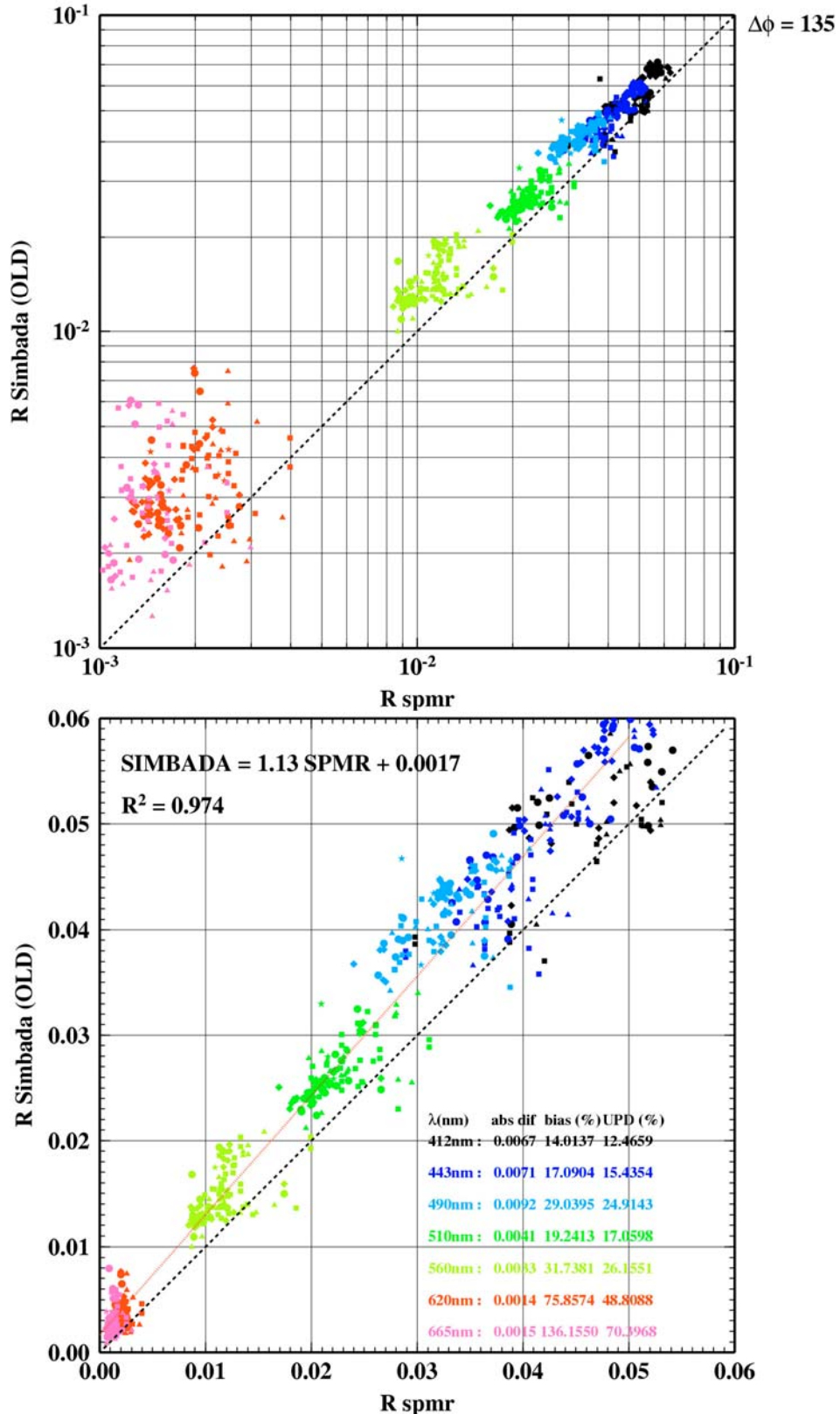
Fig. 10(a). Reflectances ($R = E_u/E_d$) derived from the SIMBADA measurements (vertical axis) *versus* reflectances derived from the SPMR&SMSR measurements (horizontal axis). Wavelengths are indicated by different colours, as indicated. The black dotted line is the 1-to-1 line and the red line is a linear regression between both data sets (equation of this regression is provided at the top of the lower panel). Diamonds are for solar zenith angles between 20° and 30°, circles for values between 30° and 40°, squares between 40° and 50°, triangles between 50° and 60°, and stars above 60°.
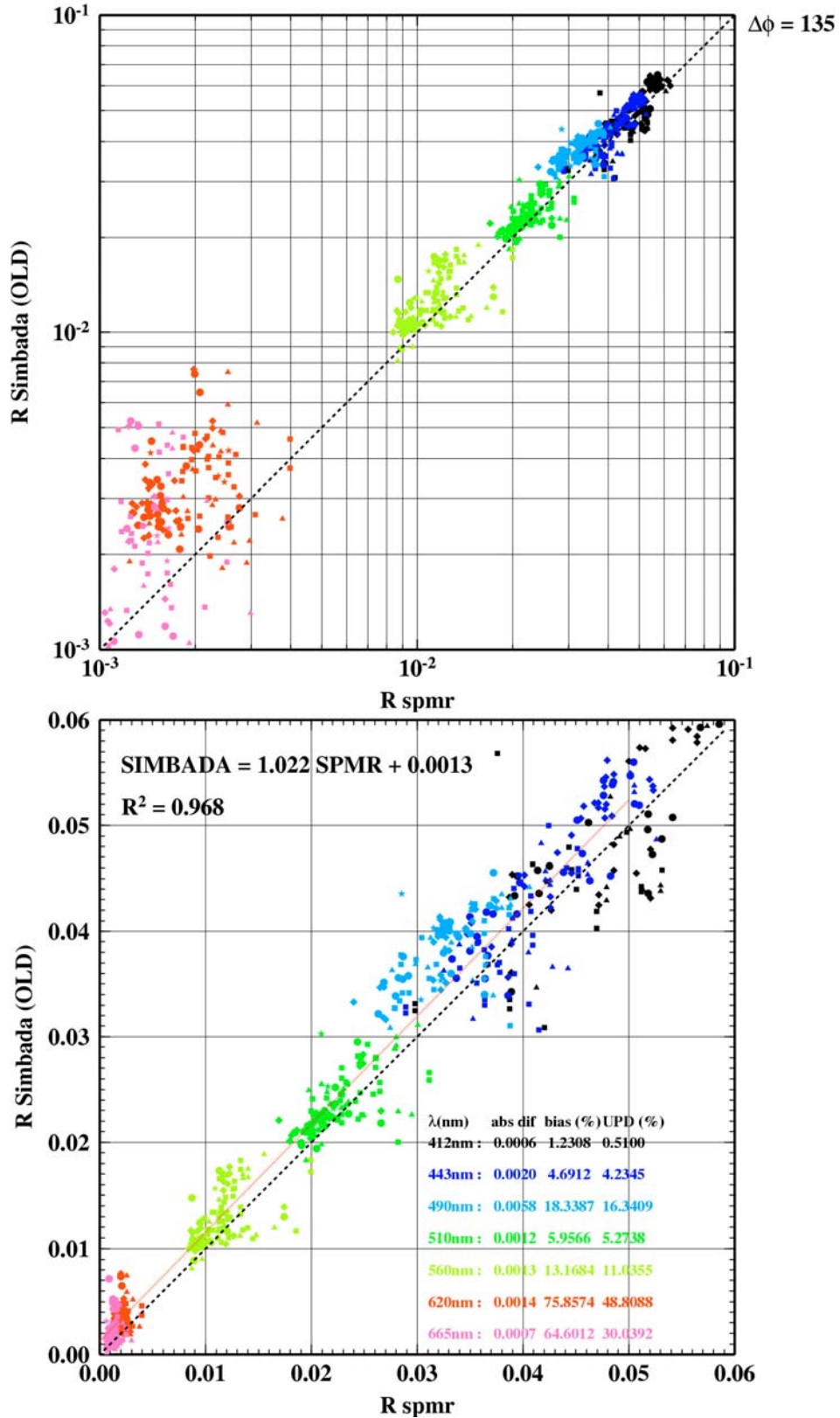
Fig. 10(b) As in Fig 10(a), but with a tentative, empirical, correction accounting for a possible residual sky light contribution into the SIMBADA measurements (*i.e.*, a further removal from the SIMBADA measurements of 60% of the diffuse sky light after it has been reflected at the sea surface, and assuming a purely molecular atmosphere).
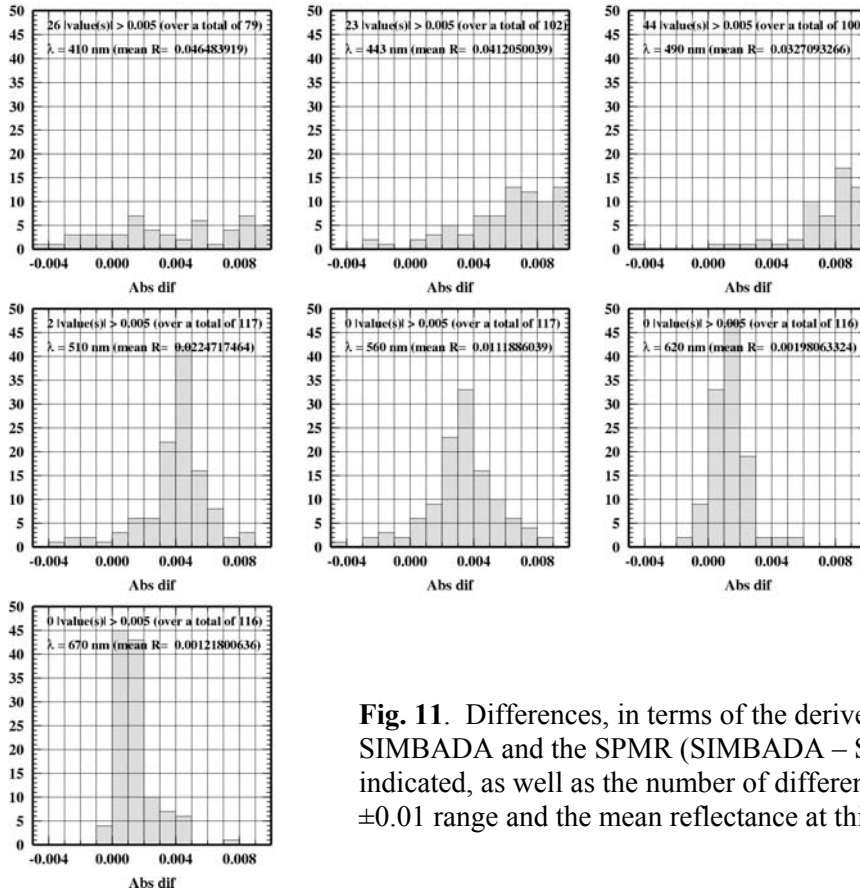
Fig. 11. Differences, in terms of the derived reflectance, between the SIMBADA and the SPMR (SIMBADA – SPMR). Wavelengths are indicated, as well as the number of differences that are outside the ±0.01 range and the mean reflectance at this wavelength.
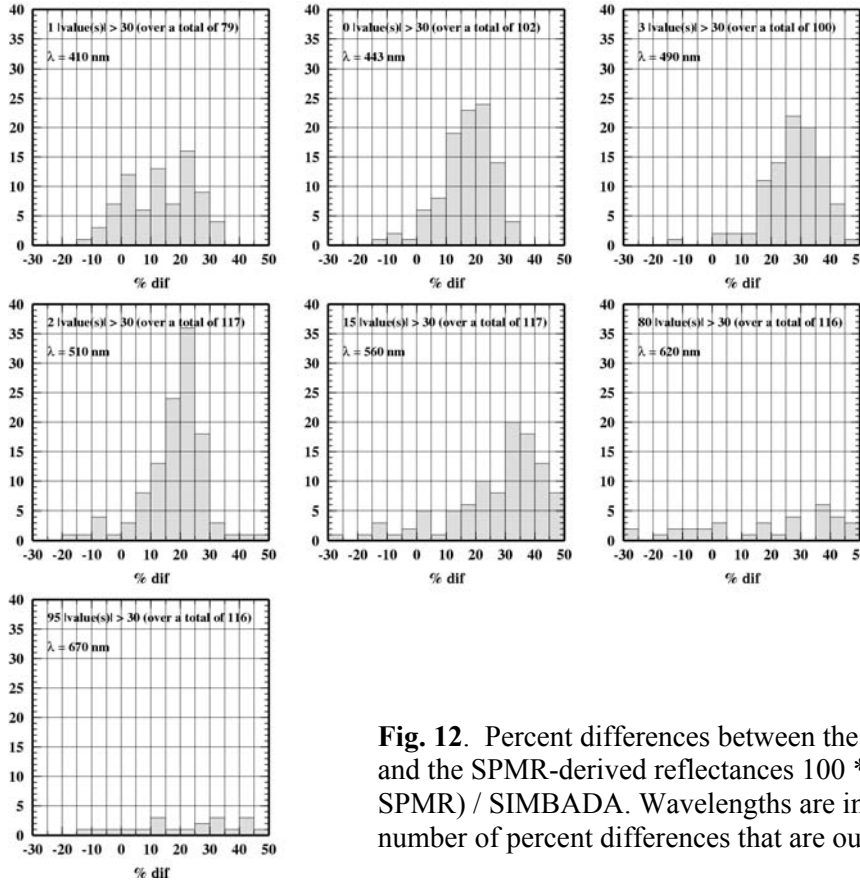
Fig. 12. Percent differences between the SIMBADA-derived and the SPMR-derived reflectances 100 * (SIMBADA – SPMR) / SIMBADA. Wavelengths are indicated, as well as the number of percent differences that are outside the ±50% range.
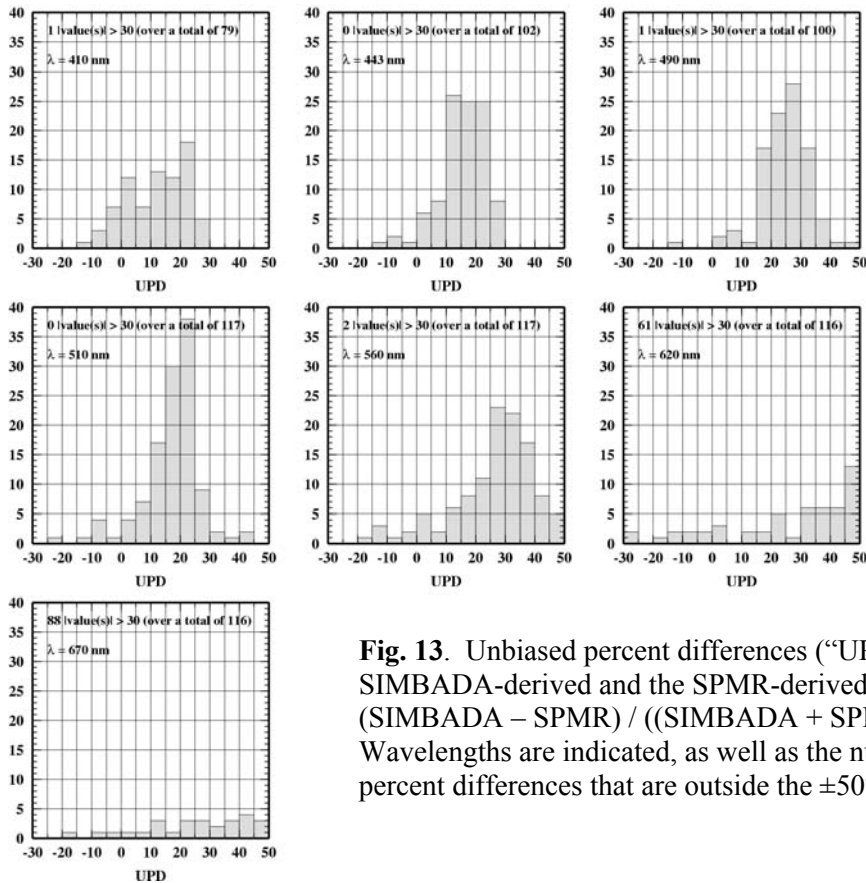
Fig. 13. Unbiased percent differences ("UPDs") between the SIMBADA-derived and the SPMR-derived reflectances 100 * (SIMBADA – SPMR) / ((SIMBADA + SPMR) / 2). Wavelengths are indicated, as well as the number of unbiased percent differences that are outside the ±50% range.
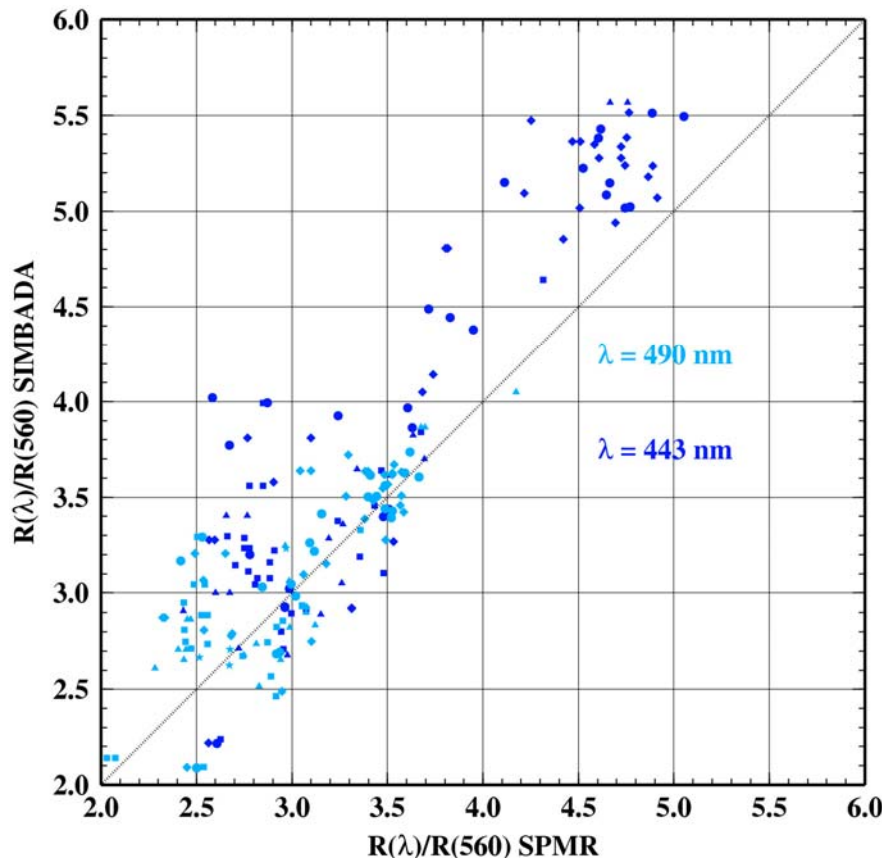
Fig. 14. Comparison between band ratios derived either from the SPMR reflectances (horizontal axis) or from the SIMBADA reflectances (vertical axis). The different symbols are as in Fig. 10, indicating various ranges of sun zenith angles. The dark blue colour is used to identify the 443/560 nm band ratio and the light blue colour for the 490 to 560 nm band ratio.
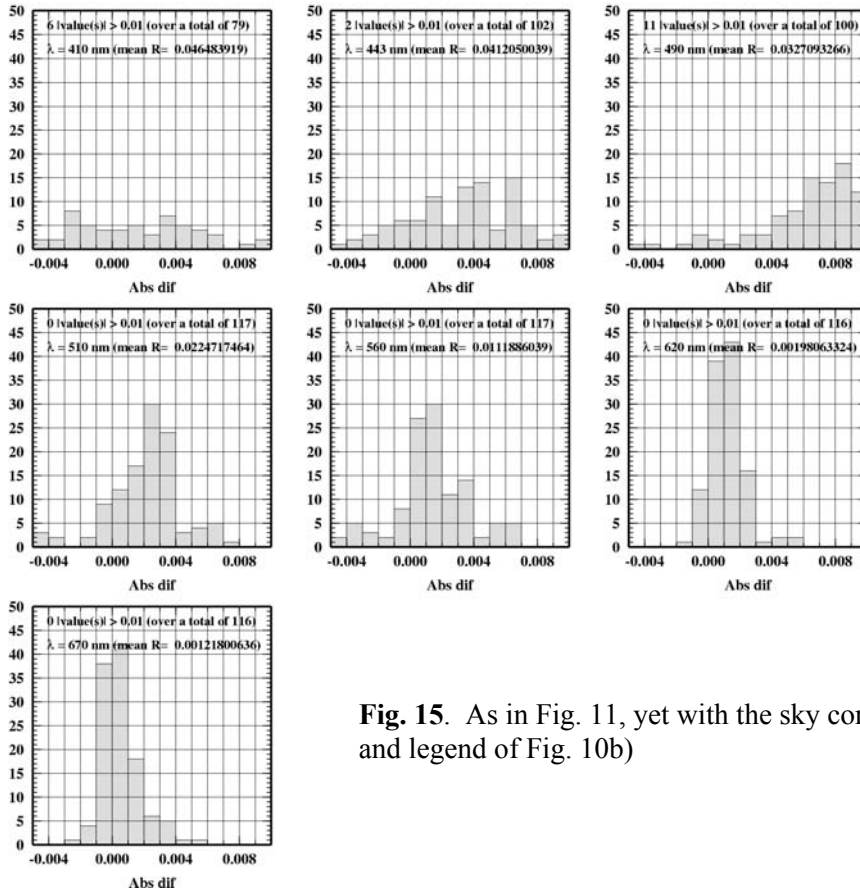
Fig. 15. As in Fig. 11, yet with the sky correction applied (see text and legend of Fig. 10b)
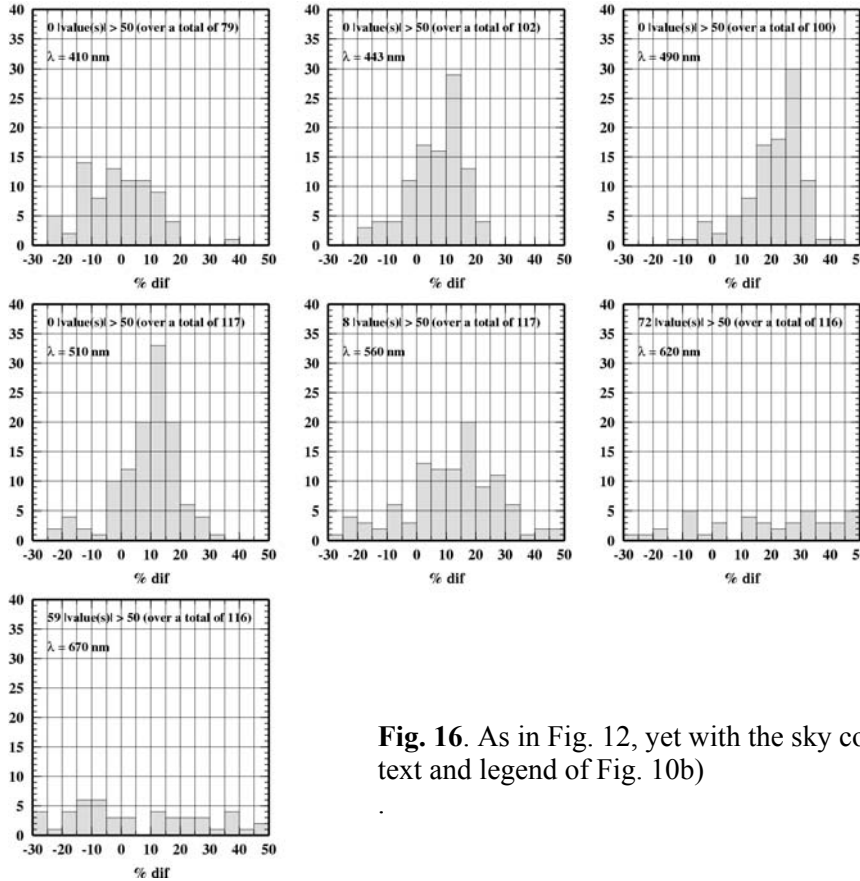
Fig. 16. As in Fig. 12, yet with the sky correction applied (see text and legend of Fig. 10b)
.
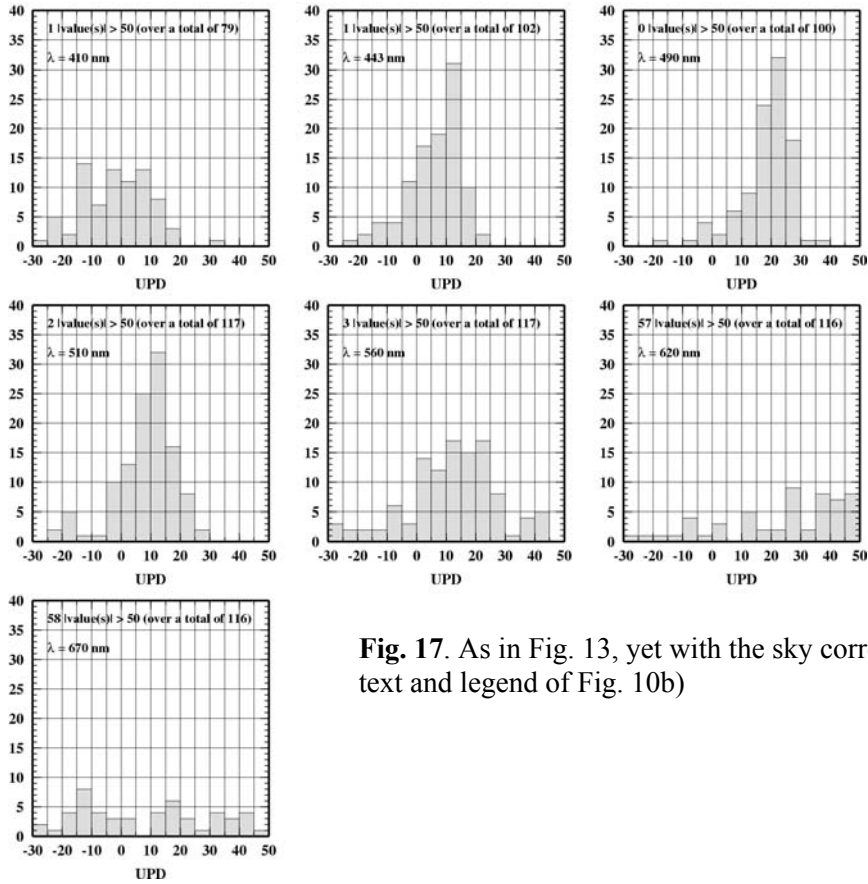
Fig. 17. As in Fig. 13, yet with the sky correction applied (see text and legend of Fig. 10b)
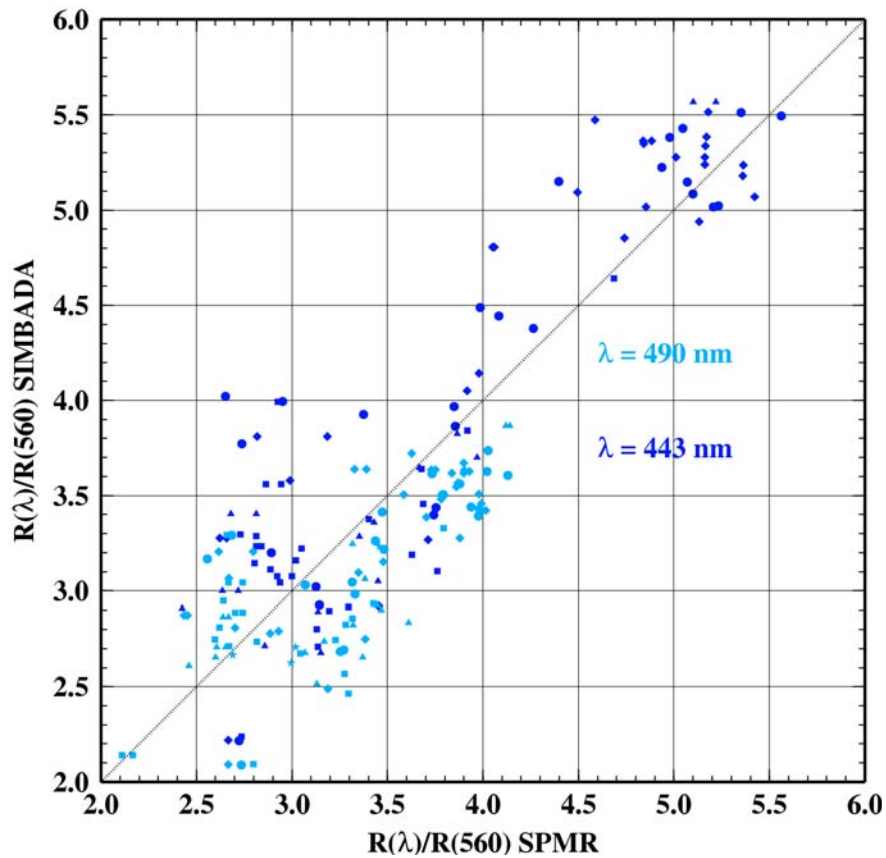
Fig. 18. As in Fig. 14, yet with the sky correction applied (see text and legend of Fig. 10b).
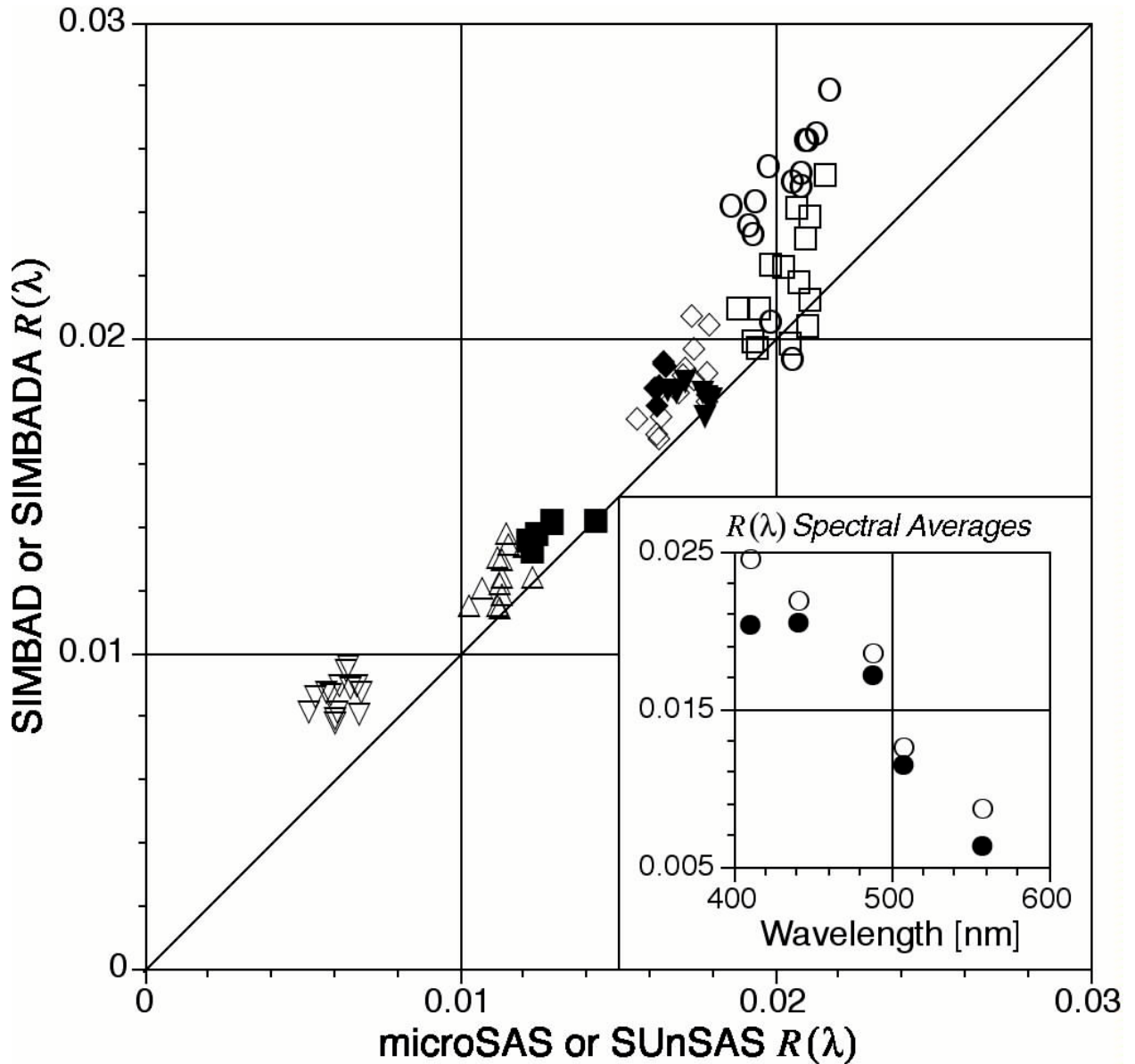
Fig. 19. (figure courtesy Stanford B. Hooker, NASA GSFC) Reflectances derived from the SIMBADA (BOUSSOLE site) and SIMBAD (AAOT site) instruments, as compared to reflectances derived from the microSAS and SunSAS instruments. The latter are using the classical protocols for above-water radiometry where the sky radiance and the downwelling irradiance are measured simultaneously to the surface reflectance (see Hooker and Morel, 2003, for the deployment techniques of these instruments, as well as section 5.3.1 of this report).

11   Appendix 1 : glossary of symbols

λ:	wavelength	nm
$L_w(\lambda, \theta_S, \theta', \Delta\phi)$:	Water-leaving radiance	mW cm^{-2} sr^{-1} μ^{-1}
$[L_w]_N(\lambda, \theta_S, \theta', \Delta\phi)$:	Normalised water-leaving normalised radiance	mW cm^{-2} sr^{-1} μ^{-1}
$F_0(\lambda)$:	Mean extraterrestrial spectral irradiance	W m^{-2} nm^{-1}
ε_c :	Correction factor applied to $F_0(\lambda)$, and	dimensionless

accounting for the changes in the Earth-sun distance.
It is computed from the eccentricity of the Earth
orbit, e = 0.0167, and from the day number D, as

$$\varepsilon_c = \left(1 + e \cos\left(\frac{2\pi(D-3)}{365}\right)\right)^2$$

$E_d(0^+, \lambda)$:	Downward irradiance just above the sea surface	W m^{-2} μ^{-1}
$K_L(\lambda)$:	Diffuse attenuation coefficient for the upward radiance	m^{-1}
$L_u(\lambda)$:	Upward radiance	W m^{-2} sr^{-1} μ^{-1}
$Q(\lambda, \theta_S, \theta', \Delta\phi)$:	Q factor (*i.e.*, E_u/L_u)	sr
$R(\lambda, \theta_S)$:	Measured reflectance just below sea surface,	
	i.e. $[(E_u(0^-) / (E_d(0^+))*0.96)]$, with a solar zenith angle θ_S	dimensionless
$\rho'_w(\lambda, \theta_S, \theta', \Delta\phi)$:	water-leaving reflectance (= $\pi L_w / E_d(0^+)$)	dimensionless
$a(\lambda)$:	Absorption coefficient	m^{-1}
$c(\lambda)$:	Attenuation coefficient	m^{-1}
$b_b(\lambda)$:	Back scattering coefficient	m^{-1}
θ_S:	solar zenith angle (cosine is μ_S)	degrees
θ_v:	Satellite viewing zenith angle (cosine is μ_v)	degrees
θ' :	$\theta' = \mathrm{asin}(\sin(\theta_v) / 1.34)$	degrees
$\Delta\phi$:	Relative azimuth difference angle	degrees
$\rho(\lambda, \theta_S, \theta_v, \Delta\phi)$	Reflectance ($\pi L / F_0 \mu_S$)	dimensionless
$\Re(\theta')$	Geometrical factor, accounting for all refraction and reflection	dimensionless

effects at the air-sea interface (Morel and Gentili, 1996)

$$\Re(\theta') = \left[\frac{(1-\overline{\rho})}{(1-\overline{r}R)} \frac{(1-\rho_F(\theta'))}{n^2}\right] \text{ (subscript 0 when } \theta' = 0)$$

where

n is the refractive index of water	dimensionless
$\rho_F(\theta)$ is the Fresnel reflection coefficient for incident angle θ	dimensionless
$\overline{\rho}$ is the mean reflection coefficient for the downwelling irradiance at the sea surface	dimensionless
$\overline{r}$ is the average reflection for upwelling irradiance at the water-air interface	dimensionless

12 Appendix 2 : individual reflectance spectra

In the following, the SIMBADA spectra are in red and the SPMR spectra are in black.
Day, month, year, GMT time and other information are provided on each panel (see also Table 1)

Each panel is duplicated, with a LOG scale (left) and a linear scale (right)

LOG Scale   LINEAR Scale

Row 1:

Plot 1: R(λ) vs Wavelength (λ) nm
7 21 2002 202 16.43 43.38 7.93 63.8 1017. 2.50 2 335. 0.258 0.356
Month day year jday H lat lon SunZen AtmP Wspeed Octa O3 taua eps

Plot 2: Month day year jday H lat lon SunZen AtmP Wspeed Octa O3 taua eps
7 21 2002 202 16.43 43.38 7.93 63.8 1017. 2.50 2 335. 0.258 0.356

Plot 3: R(λ) vs Wavelength (λ) nm
7 22 2002 203 5.47 43.37 7.91 77.5 1017. 0.90 2 335. 0.157 1.325

Plot 4: Month day year jday H lat lon SunZen AtmP Wspeed Octa O3 taua eps
7 22 2002 203 5.47 43.37 7.91 77.5 1017. 0.90 2 335. 0.157 1.325

Row 2:

Plot 5: R(λ) vs Wavelength (λ) nm
7 22 2002 203 6.60 43.36 7.90 65.3 1017. 0.90 2 335. 0.171 1.247
Month day year jday H lat lon SunZen AtmP Wspeed Octa O3 taua eps

Plot 6: Month day year jday H lat lon SunZen AtmP Wspeed Octa O3 taua eps
7 22 2002 203 6.60 43.36 7.90 65.3 1017. 0.90 2 335. 0.171 1.247

Plot 7: R(λ) vs Wavelength (λ) nm
7 22 2002 203 7.53 43.36 7.90 55.2 1017. 0.90 2 335. 0.151 1.261
Month day year jday H lat lon SunZen AtmP Wspeed Octa O3 taua eps

Plot 8: Month day year jday H lat lon SunZen AtmP Wspeed Octa O3 taua eps
7 22 2002 203 7.53 43.36 7.90 55.2 1017. 0.90 2 335. 0.151 1.261

Row 3:

Plot 9: R(λ) vs Wavelength (λ) nm
7 22 2002 203 8.27 43.36 7.90 47.3 1017. 0.90 2 335. 0.146 1.096
Month day year jday H lat lon SunZen AtmP Wspeed Octa O3 taua eps

Plot 10: Month day year jday H lat lon SunZen AtmP Wspeed Octa O3 taua eps
7 22 2002 203 8.27 43.36 7.90 47.3 1017. 0.90 2 335. 0.146 1.096

Plot 11: R(λ) vs Wavelength (λ) nm
7 22 2002 203 11.42 43.36 7.89 23.2 1017. 0.00 1 335. 0.121 1.336
Month day year jday H lat lon SunZen AtmP Wspeed Octa O3 taua eps

Plot 12: Month day year jday H lat lon SunZen AtmP Wspeed Octa O3 taua eps
7 22 2002 203 11.42 43.36 7.89 23.2 1017. 0.00 1 335. 0.121 1.336

Row 4:

Plot 13: R(λ) vs Wavelength (λ) nm
9 3 2002 246 14.30 43.37 7.89 51.7 1020. 2.50 1 307. 0.129 1.627
Month day year jday H lat lon SunZen AtmP Wspeed Octa O3 taua eps

Plot 14: Month day year jday H lat lon SunZen AtmP Wspeed Octa O3 taua eps
9 3 2002 246 14.30 43.37 7.89 51.7 1020. 2.50 1 307. 0.129 1.627

Plot 15: R(λ) vs Wavelength (λ) nm
9 3 2002 246 15.85 43.37 7.90 67.4 1018. 2.50 1 307. 0.113 1.661
Month day year jday H lat lon SunZen AtmP Wspeed Octa O3 taua eps

Plot 16: Month day year jday H lat lon SunZen AtmP Wspeed Octa O3 taua eps
9 3 2002 246 15.85 43.37 7.90 67.4 1018. 2.50 1 307. 0.113 1.661